A study of Anisotropic Conductive Adhesives with Novel Spacer Particles

by

Huyen Thanh Nguyen

Thesis submitted for the Degree of Master

Faculty of Technology and Maritime Science

University College of Southeast Norway

Spring 2016

Abstract

A method for quantitative evaluation of particle distribution, which includes clusterization and dispersion, is developed. Clusterization parameter C and dispersion parameter D were measured by statistical calculation of clusters/particles size in the matrix and sub-region particle area fraction respectively. Sensitivity of the method to different distribution patterns was high and in consistency with failure rate analytical model. This methods provides a good evaluation and classification of how well particles distribute in ACA. Results from applying the methods to real ACA bonding also show an agreement between ACA distribution and electrical failure rate.

ACAs used in this project were in paste form made of epoxy system as adhesive matrix and metal-coated polymer spheres (MPSs) as conductive particles. Spacers chosen were the uncoated polymer spheres (UPSs) made of high-crosslinked acrylic and in smaller size than MPSs. These spacers, however, cannot be incorporated directly to the epoxy matrix. Treatment of these particles is done with ethyl acetate to facilitate the wetting of epoxy on them. Spacers after treatment can be dispersed well in to adhesive and improve the distribution of particles. No short-circuit failure with gap spacing as small as $18\mu m$ is seen in bonding with spacer. Open-circuit failures still exist but can be reduced by increasing MPS volume fraction.

Spacing effects were also recognized with the similar deformation of particles under different bonding pressure. Particles were not crushed even under 18MPa. Electrical resistance also remains unchanged with increase of pressure when spacer were present. Without spacers, conductive particles were crushed under pressure of 12MPa. Although without spacers, electrical resistance is decreased with increase of pressure, the results still prove that spacers were effective in control MPS deformation.

Acknowledgements

First of all, I would like to express my to my supervisor, Professor Knut E. Aasmundtveit, for his most valuable advice and supervision. I would also like to express my sincere gratitude to Dr. Helge Kristiansen at Conpart AS for all his support and guidance.

I would like to thank my co-supervisor, Dr. Hoang-Vu Nguyen for all his constructive help and comments. Special thanks to Giang M. Nghiem for her meaningful encouragement and feedback.

I would also like to express my appreciation to the team at Conpart AS, Erik Kalland, Susanne Helland and Dr. Keith Redford for providing materials and help me with manufacturing the adhesives.

I am especially grateful to Zekija Ramic, Ragnar Dahl Johansen and Anh-Tuan Thai-Nguyen for their invaluable help and contribution to my fabrication processes. I also thank the Faculty of Technology and Maritime Sciences, and particularly to the Department of Micro and Nano Systems Technology for their most useful facilities and invaluable administrative assistance.

I would also especially like to thank my friends for their valued friendship and encouragement during the period of my project. I greatly appreciate Dr. Cuong Phu Le for his precious comments and advices.

Finally, I am very grateful to my family, who always loves, understands and encourages me to do my very best. They are my motivation for all I have been doing.

May 2016
Huyen Nguyen

Contents

Acronyms

ACA	Anisotropic conductive Adhesive
LCD	Liquid crystal display
ACP	Anisotropic conductive Paste
ACF	Anisotropic conductive Film
MPS	Metal-coated Polymer Sphere
UPS	Uncoated polymer sphere
TAB	Tape Automated Bonding
TCP	Tape Carrier Package
IC	Integrated circuit
COG	Chip on Glass
COF	Chip on Flex
NCA	Non-conductive Adhesive
ICA	Isotropic Conductive Adhesive

Chapter 1

Introduction

Anisotropic conductive adhesives are widely used in LCG packaging for its advantages: fine pitch capability, low bonding temperature, elimination of underfill, process simplicity and flexibility, and low cost [1]. ACA consists of an adhesive polymer matrix filled with conductive particles. These particles, usually metal-coated polymer spheres (MPSs), are trapped and compressed between bumps and corresponding pads, providing vertically electrical conduction paths while insulates horizontally in xy-plane.

Deformation and distribution of particles in interconnects play a crucial role in ACA performance. Although has been developed strongly since its invention in 1970s, the problem relate to controlling particle deformation of ACA in industrial applications still exists. Furthermore, a tool to quantify the particle distribution is essential but has not been develop fully for ACA applications. In this thesis research, a new solution for control particle deformation was proposed, which is incorporation of small non-conductive particles (called spacers) of size close to the desire deformation. To evaluate the ACA quality, as well as the effect of spacers on conductive particle distribution, a quantification method was developed. Together with this quantification tool, a random-like distribution model was also created, which would be the standard for evaluating and classifying ACAs' quality.

The main goal of this master thesis has been to study the effect of spacers on the ACA bonding, including their influence on MPS distribution and deformation. In order to achieve this, several works were need to carried out: developing a

quantification tool to evaluate MPS distribution (disccused in chapter 3), mixing of ACA (section 4.1), design and fabrication of testing devices (section 4.3 and 4.4), bonding and evaluate particle deformation (results are shown in 5).

Chapter 2

Background and motivation

2.1 LCD packaging

Liquid-crystal displays (LCD) are currently the dominance of electronic visual displays at all sizes and levels. It has a vast range of applications, including televisions, computer monitors, mobile phones, etc. and has replaced CRT almost completely. In mobile devices, it is of necessity to have a display which is small, light weight and high energy efficiency [2]. Thus, packaging technology has a significant influence on performance of the display, and can be the dominant differentiator for some applications [3].

Traditional LCD modules involve tape carriers packages (TCPs) that packaging and interconnect driver circuit to LCD cells using a tape automated bonding (TAB) process (figure 2.1a). The technology becomes outdated due to its dimensional incapability of meeting modern LCD packaging demands [4]. The trend of display technology is to have better resolution, thus more interconnects, in a smaller package size balanced with cost and manufacturing process [3]. Therefore, chip on flex (COF) and chip on glass (COG) technology using anisotropic conductive has been introduced. In COG, integrated circuit (IC) packing has been eliminated entirely since the driver is mounted directly onto the display module (figure 2.1b).

Several approaches for COG attachment have been developed, including die and wire bonding, low temperature alloy soldering, transfer printing of isotropic conductive adhesive (ICA), bump bonding with non-conductive (NCA) or anisotropic

conductive adhesive (ACA) [3]. Apart from die and wire bonding, all other techniques involve a flip-chip bonding process where the bare chip is face-down (flip) and mounted directly to the glass substrate. Although has been well proven for its reliability, wire bonding is not suitable for LCD packaging because of its high cost, long processing time and large device footprints. Soldering and ICA, which do not have capability for fine pitch applications and require underfill adhesive, are not widely used either. Therefore, flip-chip bonding using NCA or ACA is currently the most common technology for LCD packaging and is still developing. Next section will discuss in detail this technology.

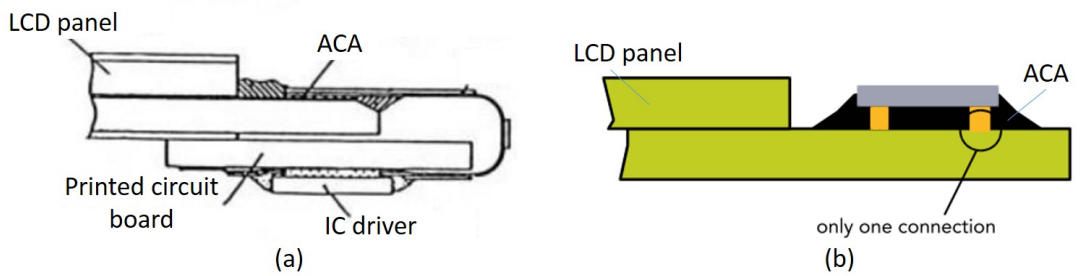

Figure 2.1: LCD's packaging technologies - (a) Cross-section of tape carrier package (TCP). IC driver is bonded to TAB tape and packaged, forming a TCP. The package is then bonded to the display glass using Anisotropic Conductive Adhesive (ACA) and subsequently attached to circuit boards using solder or ACF. [5]. (b) Chip on glass packaging. A non-packaged chip driver is mounted directly to the display glass, only one interconnection (from IC to LCD) is needed. [6]

2.2 Flip-chip bonding technology using adhesive

Flip-chip bonding is defined as a bonding process in which a non-packaged chip is turned upside down (flip-chip) and bonded directly to a printed circuit board or chip carrier substrate [7]. Flip chip bonding using adhesive is widely used in temperature sensitive application and has been being strongly developed. First type of adhesive, anisotropic conductive adhesive (ACA) comprises of conductive particles dispersed in an polymeric adhesive matrix. The other type, non-conductive adhesive (NCA) is only a polymer matrix without any conductive particles. [4]

Figure 2.2 and 2.3 show the conducting principle of ACA and NCA respectively. In ACA flip-chip bonding, conductive particles, usually metal-coated polymer spheres (MPSs), are trapped and compressed between bumps and corresponding pads that allows vertically electrical conduction while insulates horizontally in xy-plane. On the other hand, in NCA bonding process, bumps are in direct contact with corresponding pads. In both types, the adhesive matrices used are usually thermosetting polymers which are cured under high temperature and secured the connection formed between bumps and pads.

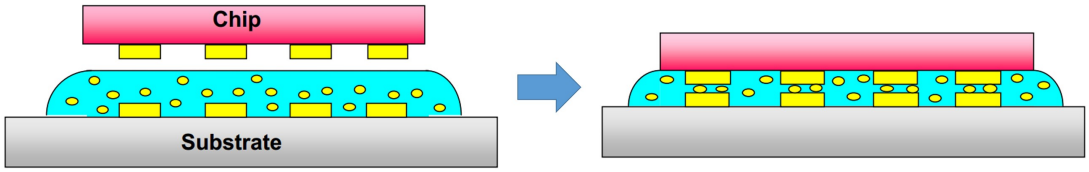

Figure 2.2: Schematic diagram of ACA bonding [8] - Conductive particles are trapped, deformed and conduct between bumps and pads while isolated by adhesive matrix between neighbor bumps

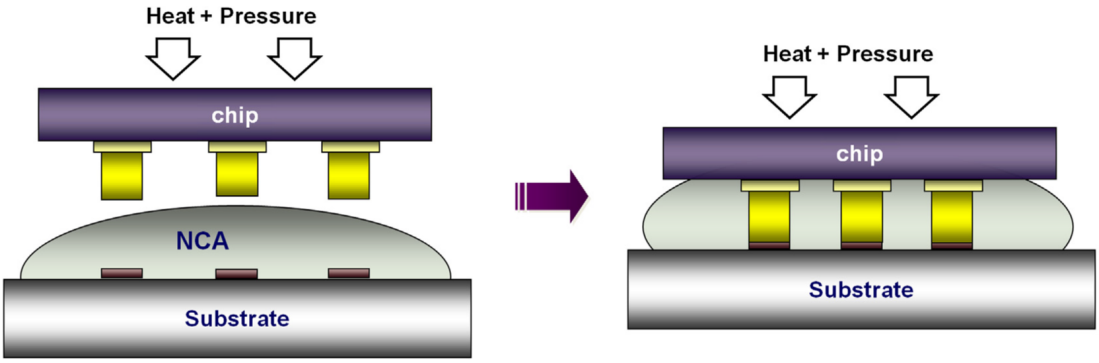

Figure 2.3: Schematic diagram of NCA bonding [4] - Bumps on chip and pads on substrate are in direct contact

In NCA bonding, the lack of compliant particles makes the bump fabrication process and material selection become crucial. The bumps should be deformed easily to compensate the bump height variations. The shapes and surface roughness of the bumps can also affect the contact area due to adhesive matrix entrapment. Soft metal bumps such as Sn, Cu/Sn bumps or Cu pillars are mainly used for NCA bonding. Contact problems and reliability issues still remain a

great concern with metallic bump NCA bonding. The resin core bump technology (figure 2.4) [9], however, had overcome these limitations, thus ultra-fine pitch size can be achieved and reliability can be improved. The technology could reach $5\mu m$ if the fabrication of metal line is possible.

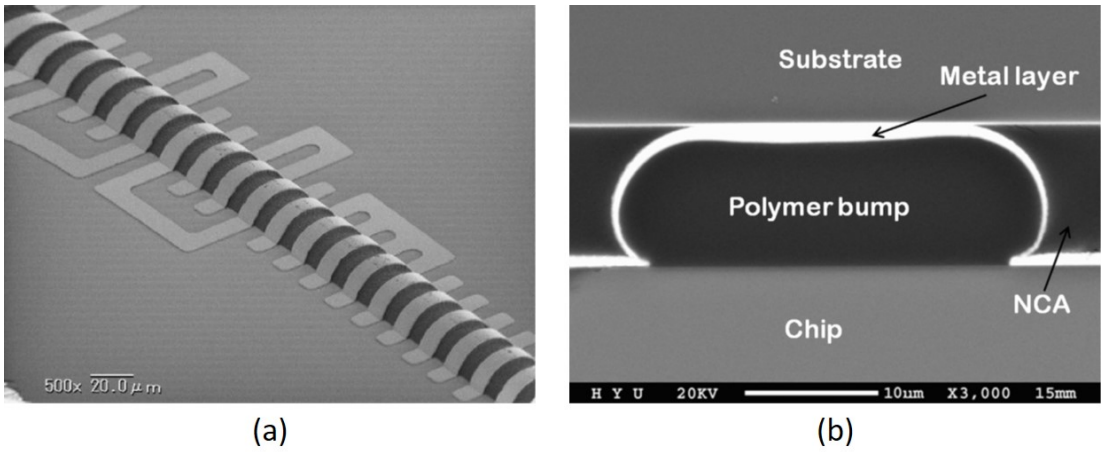

Figure 2.4: SEM images of resin core bump- (a) A resin core bump with metal electrodes of pitch $20\mu m$ [9]; (b) Cross-section shows bump's hemispherical topology, the bump was deformed and contacted to the substrate [4]

Issues relating to ACA for filp-chip bonding is the trade off between width of a bump and spacing between bump pairs, corresponding to the vertical interconnect resistance and horizontal bump insulation respectively. This may hider the performance of ACA with short circuiting between neighbor bumps and open circuit between bumps and pads. Several solutions have been proposed [10–14] to overcome these problems. In study of Yim et al [10], double layered anisotropic conductive adhesive film (ACF), one with non-conductive filler. Hong et al [12] cover the bump walls with photo-resist. These improvements were evidenced to had decreased short circuit rate and improve number of trapped particles. K.Lim Suk and S.Hoon Lee et al [13, 14] introduced Nanofiber Anisotropic Conductive Films, where conductive particles were coated and tied by nanofiber, that in the same time prevented from direct contact of the particles but also trapped more particles. The finest pitch ACA could reach from the studies was $20\mu m$, with gap spacing between bumps of $8\mu m$.

Compared to NCA, which does not have electrical short problem, ACA is not capable of accommodate as small pitch. However, strict requirements in chip fabrication for NCA technique and high pressure in bonding have restricted the applications of NCA. Nowadays, flip-chip using ACA still remains the most popular interconnection technology in LCD packaging industrial.

2.3 Anisotropic conductive adhesive

ACA as mentioned consists of an adhesive polymer matrix (usually thermosetting) and conductive particles. The concentration of particles can vary from applications and types of ACA, but is always keep far below the spherical percolation threshold to prevent contact between particles. During bonding, many process take place, including flowing of the adhesive, which fill the space between and outside bumps, trapping and deforming conductive particle and curing of adhesive. Curing process happens under high temperature, after that the adhesive is harden and particle deformation, which facilitate conduction of ACA, is maintain. Two typical failure modes of ACA are: short-circuit between neighbor bumps and open or insufficient connection between bumps and pads (Figure 2.5).

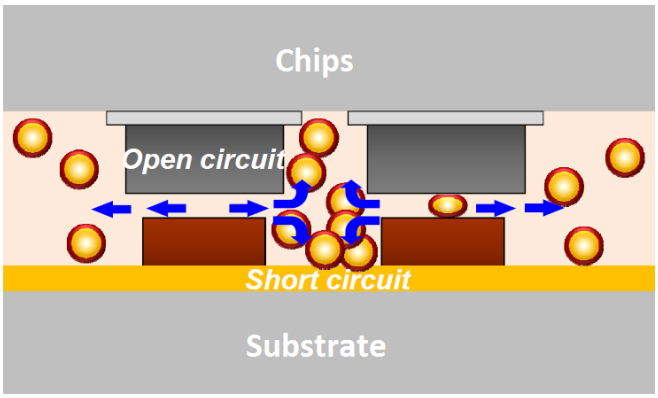

Figure 2.5: Failure modes of ACA: open circuit and short circuit

Particles in ACA can be massive conductive particle such as graphite or metal (gold or silver) particles, massive polymer particle coated with conductive material and hollow polymer particle coated with conductive material. The most used particle type is metal-coated polymer sphere (MPS). With the compressibility and elasticity, particles of this type provide large contact area, flexibility and

safety in connection. MPS size is mono-dispersed and varies from 3 to $10\mu m$, the the finer the pitch is, the smaller the particles must be. An advanced form of MPS was also introduced, having an additional insulating layer ($\sim 10nm$ thick) to prevent short-circuit failure [15].

Properties relating to adhesive matrix play crucial roles in ACA bonding. Viscosity of resins, mechanical properties after curing, adhesion to bonding substrates, and degradation of polymer is decisive to electrical resistance, mechanical strength and reliability of ACA flip-chip interconnection. The most common polymer type used for adhesive matrix in ACA is an epoxy system, including an epoxy resin and hardener agents. Anisotropic conductive adhesive exists in two forms: paste (ACP) and film (ACF). In ACP, liquid form of epoxy is used with latent curing systems to prevent ACP from early curing in storage. ACF on the other hand has a solid epoxy matrix, which is only cured when it is melted. ACF is widely use in LCD packaging for it better controllability of adhesive filling process and particle distribution compared to ACP form.

Although paste form of ACA can introduce some problems due to the flow of the paste in bonding process, it is still a useful testing vehicle when incorporate new particles prior to ACF production. Compared to ACF, ACP has lower cost and simpler bonding process. With the availability of screen and jet printing, ACP still also has many application in industry.

Typical flip-chip bonding process of an ACF: 1) ACF chip-size cutting; 2) ACF pre-lamination on a substrate; 3) removal of releasing film; 4) alignment of the chip and substrate; and 5) flip-chip interconnections by thermo-compression bonding [16]. ACP bonding reduces chip-size cutting, and removal of releasing film steps. The bonding parameters that can affect the final quality of bonds are: bonding temperature, pressure, and time and accuracy of alignment [17]. Several studies has been carried out to optimize the bonding parameters [18–20]. This study has not focused on bonding parameters, instead, a workable bonding process was found and keep the same during the whole study.

Electrical resistance of final ACA interconnection depends on: surface of the connecting bumps and pads, the metal layer of MPS, the number of trapped particles, and deformation of MPS. The first two factors are related to the manufacturing of components and MPS. Number of trapped particles is affected by many parameters such as volume fraction and distribution of MPS in ACA, flowing of

adhesive matrix in bonding process, the form of ACA, etc. Therefore, number of particles trapped on a bumps in ACA bonding usually vary considerably.

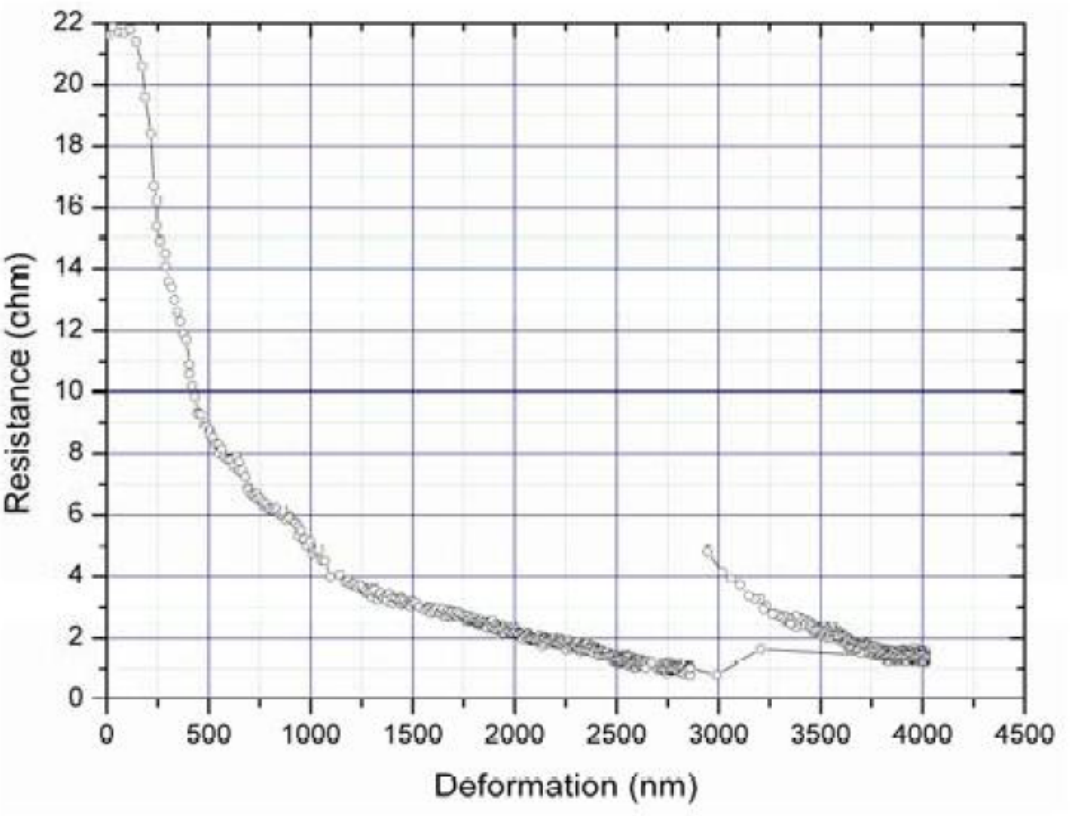

Figure 2.6: Effects of deformation on resistance of single particle [21] - The resistance was measured on a single particle of size $5.75\mu m$, joining W/Cu (60/40) flat punch and brass base stage

Deformation of particles mostly depends on bonding pressure and co-planarity between planes of bump and pad surface. Figure 2.6 shows the effects of deformation of a single particle on its resistance. As can be seen, the resistance decrease greatly with the increase in particle deformation until 2750nm, where particle started to crush. Further deformation also decrease the resistance. However the crushing of polymer core and separation of metal layer that might introduce reliability problems is unwanted. With the variation of number of trapped particles and co-planarity problem, the perfect and uniform deformation of particles in bonding is difficult to achieve. In this study, a new solution for controlling de-

formation of particles has been introduced to be incorporation of non-conductive particles called spacers. These spacers were smaller than conductive particles and could act as mechanical stop between bumps and pads thus restrict the deformation of MPS to some certain range around the spacer size.

Non-conductive particles had been introduced into ACA for different purposes: silica fillers had been incorporated into ACF to improve reliability by control the coefficient thermal expansion (CTE) of the adhesive [22], small non-conductive particles (with size of one fifth of MPS size) was added to prevent electrical short of ACA [10]. This study carried by Yim et al [10] also showed an influence of non-conductive fillers on trapping of MPS. There is still no publication about using non-conductive particles as spacer for controlling conductive particle deformation. Non-conductive particles chosen as spacers in this study were polymeric particles in order to avoid damaging the surface of metal coated particles as well as the bonding bumps and pads.

2.4 Adhesion mechanism

The adhesion mechanism of an adhesive is discussed in details in [23]. To form adhesion with a solid surface, the adhesive must first make intimate, molecular contact with the substrate surface, i.e "wet" the surface. Permanent adhesion results primarily through forces of molecular attraction.

Wetting of adhesive to the adherent surface provides contact area over which adhesion force may act. For good wetting, the surface free energy (surface tension γ_{LV}) of the liquid adhesive must be less than that (critical surface tension γ_C) of the solid adherend. $\gamma_{LV} < \gamma_C$

Low-energy polymers, therefore, easily wet high-energy substrates such as metals. Conversely, polymeric substrates having low surface energies will not be readily wet by most other materials. The fact that good wetting requires the adhesive to have a lower surface tension than the substrate explains why organic adhesives, such as epoxies, have excellent adhesion to metals, but offer weak adhesion on many untreated polymeric substrates..

The wetting mechanism also plays important role in mixing of particles into polymer matrix. For proper dispersion of particles, the polymer adhesive must first wet the surface of particles before separate them from each other. Poor

wetting leads to presence of large particle clumps and non-uniform particle concentration in the adhesive matrix.

Chapter 3

Distribution quantification

3.1 Introduction

Distribution of particles in the matrix plays a significant role in the electrical properties of bonding using ACAs. Distribution of particles in the matrix includes two phenomena: clusterization and dispersion. Clusterization is the trend of particles to stick together, randomly or by attractive forces such as Val der Waals force or electrostatic force. Dispersion, on the other hand, indicates the uniformity of spreading out those clusters over the space. First phenomenon is mainly caused by particles and their separation process while the other mostly depend on the matrix and its spread out process. Two typical failure modes of ACA bonding exist: short-circuits between adjacent bumps and open-circuit within interconnects. Clusters of particles with size larger than the minimum spacing between bumps can cause short-circuits while a non-uniform dispersion might lead to the latter failure mode. Thus, distribution of these particles in the matrix plays a significant role in ACA fine/ultra-fine pitch applications. A tool to quantify the particle distribution is therefore essential for characterization of the ACAs prior to the bonding process.

Several methods have been proposed for quantifying nano-particle distribution in composite materials [24–28]. A dispersion parameter called Area Disorder was used by David J. Bray, et al [24] to quantitatively classify the dispersion of particles as good, random or poor. Images of the material was divided into a triangle network, where each vertex of a triangle was a particle and no particle

was found inside a triangle or on its edge. An Area Disorder was then defined based on the ratio between mean of triangle areas and their standard deviation. This method however did not provide any evaluation on agglomeration of the particles.

Luo & Koo [25] calculated dispersion quantity D based on measurement of distances between particles. D was a percentage value, higher D meant better dispersion of particles. B.M. Tyson et al [27] improved the method by adding quantification of agglomeration. Characterized properties were the size of fillers/clusters and distances between them in x and y direction. The method proposed by T.Glaskova et al [28] focused on studying the agglomeration/ clusterization of particles by similar calculation on area of clusters. Since distribution parameters quantified were percentage values, these methods can provide a good insight of how well filler particles disperse or agglomerate into the composite matrix.[27]

However, short-circuiting in ACA bonding is caused by clustering of particles in any direction. Study of cluster size in one direction or cluster area does not related directly to possibility of this failure. Similarly, distances between particles only have a weak relation to open-circuit failure. Therefore, in order to utilize these methods in evaluation of ACA particle distribution, further improvement was needed to be made.

3.2 Methodology

3.2.1 Previous quantification methods

Figure 3.1 describes the procedure of obtaining dispersion parameter D_k and agglomeration parameter A_k suggested in [3] and [4]. A grid-line network in x and y direction was first created on the image under consideration. Data of white segments on the grid-lines was recorded as free-path spacing x_D while black segments represented filler agglomeration sizes x_A. Histograms of the two data sets (x_D and x_A) were plotted and fitted to either normal or lognormal distribution. From the fitted curve, a probability density function $f(x)$ was obtained and the dispersion parameter D_k and the agglomeration parameter A_k were calculated.

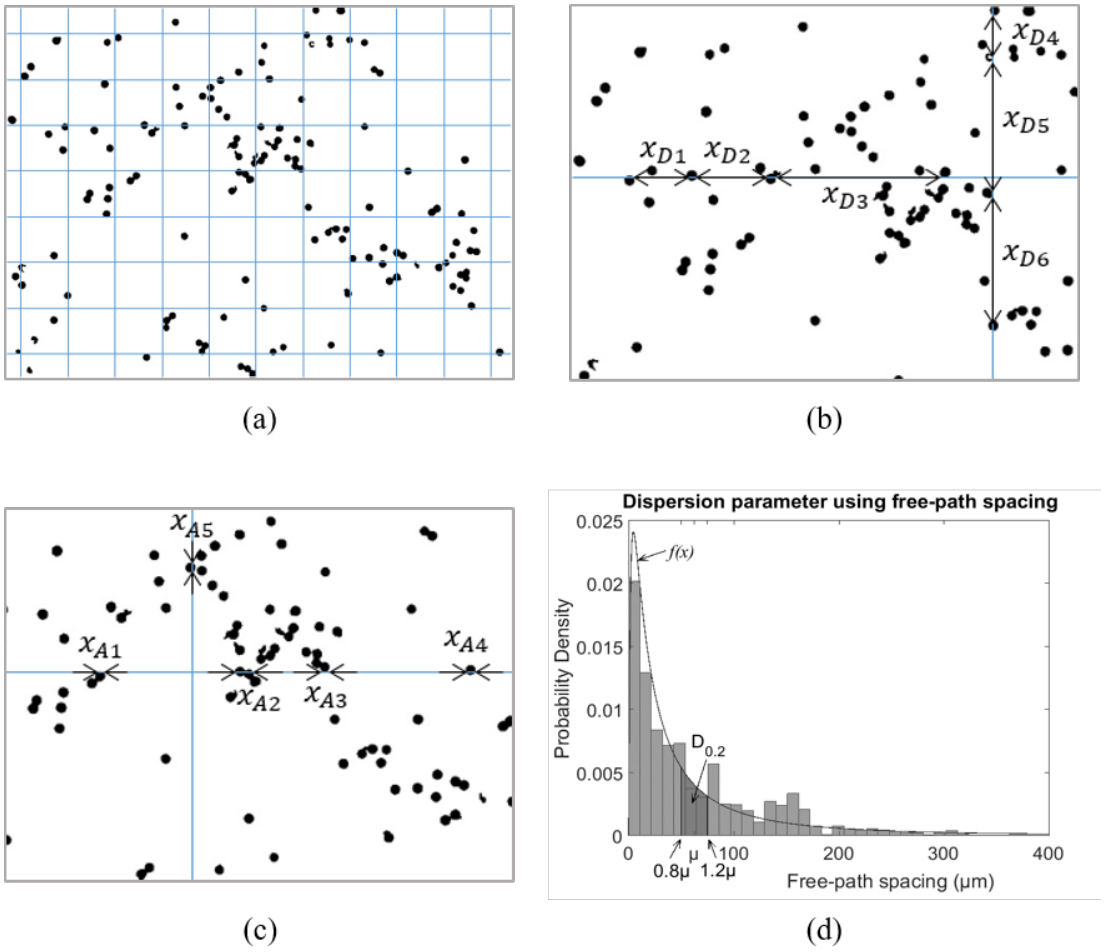

Figure 3.1: Determination of distribution parameters - First, a gridline network was made on the image (a). On each line, white segments representing particle spacing (b) while black segments represent particle sizes were measured and histogram of them were plotted. In (d), histogram of particle spacing was plotted and a lognormal curve were fitted. $D_0.2$ was the shaded area under the fitting curve, where μm was the mean value of particle spacing.

D_k and A_k were related to the probability of x falling in a certain range k around the mean value μ of x, i.e. the integration of $f(x)$ from $(1-k)\mu$ to $(1-k)\mu$:

$$D_k = \int_{(1-k)\mu_{x_D}}^{(1-k)\mu_{x_D}} f(x_D)dx_D \tag{3.1}$$

$0 < k < 1$ and k was chosen in such way that $f(x)$ in the considered range was linear. We have:

$$\int_0^\infty f(x)dx = 1 \tag{3.2}$$

Therefore, $0 < D_k < 1$ and $0 < A_k < 1$. B.M. Tyson et al [4] proved that the larger D_k is, the narrower the statistical distribution of x_D is, thus the more uniform the dispersion of fillers in the matrix is. While A_k was set up in such a way that smaller A_k indicated less agglomeration.

T.Glaskova's work [5] focused on studying the agglomeration/clusterization of particles by similar calculation on areas of clusters. Normal distribution was fitted to the data.

3.2.2 A modified method for ACA application

There exist very few published works on the particle distribution in ACA. Therefore, a tool for quantifying and evaluating ACA particle distribution is of apparent necessity. In this work, a method for quantification of mono-sized particle distribution in an adhesive matrix was adapted from previous methods with improvement and modification. For sufficient quantifying the distribution of ACA particles, there is a need of analyzing both parameters for clusterization and dispersion of the particles.

Non-uniform dispersion of the particles/clusters may lead to areas with insufficient particles to conduct in z-direction. Free-path spacing property as in mentioned methods can be used to characterize dispersion of particles. However, in order to fit better the requirement of ACA, a different property was proposed when quantifying dispersion parameter, which was the sub-region area fraction a. A shaded rectangle in Figure 3.2 represents a sub-region of interest, which can

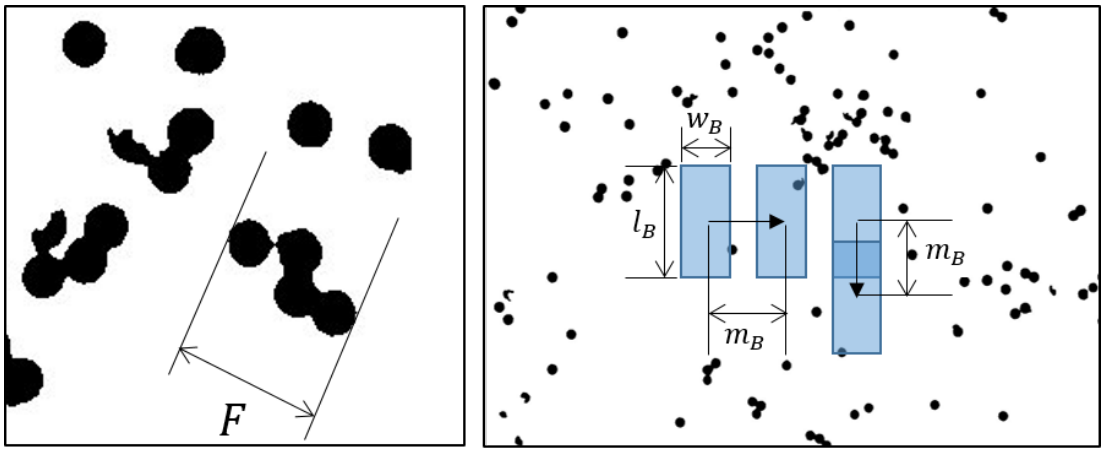

Figure 3.2: Determination of Feret diameter F and sub-region area-fraction a - (a) Cluster size F was the maximum Feret diameter, i.e. the maximum distance between the two parallel planes restricting the cluster perpendicular to that direction. (b) Sub-region area fraction a was the particle covered area fraction in a small area defined by the grey rectangle with dimensions $l_B \times w_B = 15\phi \times 3\phi$. This grey rectangle was moving through the whole area of the image with step $m_B = \phi/3$, collecting data of a.

be consider as a bump to connect. Area fraction a on this bump was the ratio between particle covered area over the area of the bump.

$$a = \frac{\text{Bump area covered by particle}}{\text{Total bump area}} \tag{3.3}$$

This bump of dimensions $15\phi \times 3\phi$ was moving with a small step m_B through the whole image, collecting area fraction a in each position. Histogram of recorded data is plotted in Figure 3.3 indicating how uniform the area fraction a was over the whole image. Similar to previous method, the dispersion parameter D_k was related to the statistical distribution of sub-region area fraction a. However, since the ACA particle distribution had not been studied carefully, it was not reasonable to fit the statistical distribution of a to any laws of distribution in advance. Therefore, the discrete histogram (Figure 3.3) of real measured values was used to extract D_k, which was then defined as the ratio of total number of a fall in the range of $(1-k)\mu_a$ to $(1-k)\mu_a$ over total number of data collected, where μ_a was the mean area fraction.

$$D_k = \frac{\sum_{(1-k)\mu_a}^{(1+k)\mu_a} N(a)}{\sum N(a)} \tag{3.4}$$

$0 \leq D_k \leq 1$ and D_k can be expressed as a percentage value. $D_k = 1$ means perfectly uniform dispersion of particles while $D_k \approx 0$ means area fraction in the sample differ significantly from one place to another.The larger D_k is, the better the uniformity of spreading particles over the matrix is.

Dispersion parameter does not take into account the clusterization of particles that cause short-circuiting failure. For quantification of clusterization, clusters and cluster size were first defined. A cluster was defined as a group of particles having physical contacts that can provide continuous conduction paths from any particle to all the other particles within the group. The size F of a cluster was its maximum Feret diameter, where Feret diameter was the distance between two parallel tangents on opposite sides of the cluster [29], as shown in Figure 3.2. Thus, two neighbor bumps with spacing smaller than size of a cluster would have a possibility of being short-circuited by that cluster. Separated single particles were considered as clusters with size equaled to their diameter. Since this study has focused on mono-sized particles, the cluster size unit was one particle diameter, denoted as ϕ.

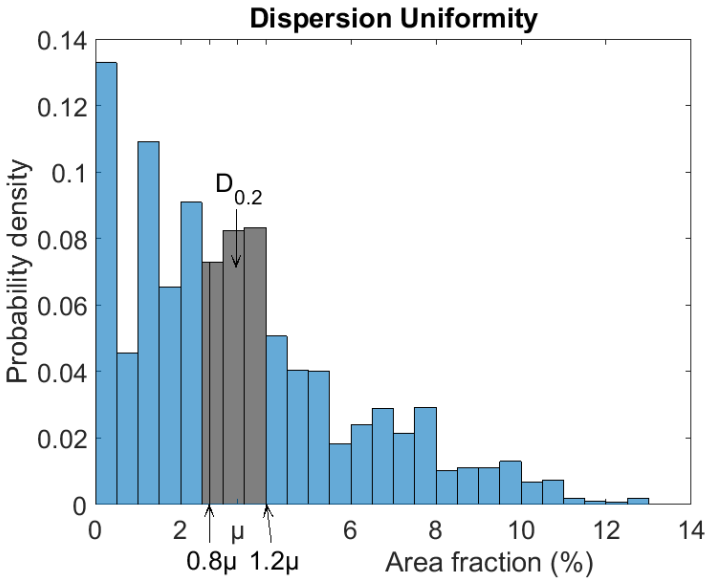

Figure 3.3: Dispersion parameter definition based on sub-region area fraction a

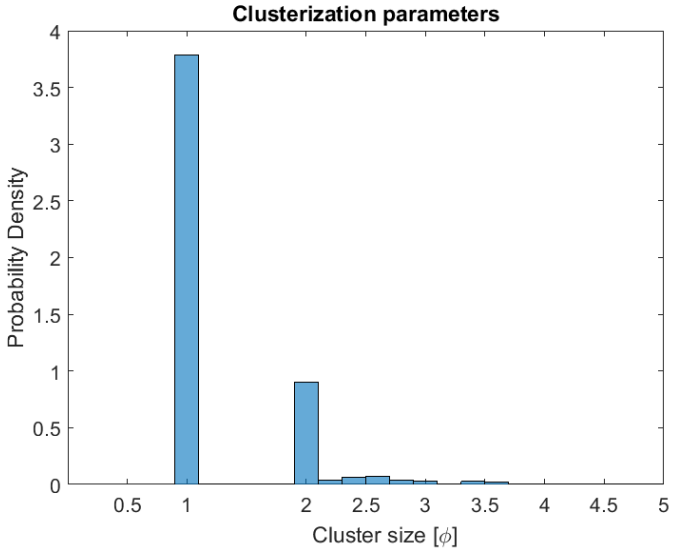

Figure 3.4: Original cluster size histogram

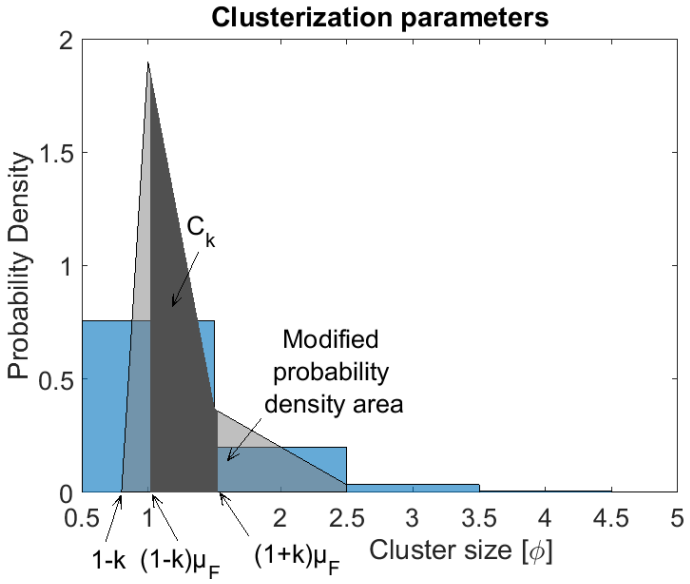

Figure 3.5: Clusterization parameter definition

To quantify the degree of particle clustering, approach similar to that of D_k could be use as in equation refeq:ck1.

$$C_k = \frac{\sum_{(1-k)\mu_F}^{(1+k)\mu_F} N(F)}{\sum_0^{F_{max}} N(F)} \tag{3.5}$$

However, since mono-sized particles were to be focused on, there would be no cluster size fall between 1ϕ and 2ϕ, as shown in the original histogram of F (figure 3.4). If $1.25 < \mu_F < 1.6$, C_k from eq.3.5 would equal 0. This will make a false indication of particle clusterization. C_k was modified by adding a condition that if $\mu_F < 2$, where μ_F was the mean cluster size, then C_k would equal the shaded area in figure 3.5. The modified probability density was obtained by making the area be continuous through non-integer size but reserve the total area and assume the linear trend of decrease probability density with increase of cluster size.

$0 \leq C_k \leq 1$ and C_k can be expressed in percentage value. For ACA application, where the area fraction of particle is mainly smaller than 15%, most of clusters in an image are single particles and mean cluster size μ_F is close to 1ϕ. The existence of large clusters increases μ_F further from 1ϕ as well as widens the statistical distribution of cluster size, thus considerably decreases C_k. An image with only single particles has $C_k \simeq 0.75$ (due to the modified area in figure3.5)

while $C_k \approx 0$ if an image contains clusters with size varying greatly. Therefore, C_k can express well the degree of particle clustering, the larger C_k is, the less clustering between particles is.

3.3 Failure rate: analytical calculation

Two-dimensional situation with mono-layered conductive particles was considered. Open-circuit are caused by lacking of conducting particle on a flat bump area and short-circuiting was resulted from cluster with size larger than gap spacing between neighbor bumps. Williams and Whalley [30] has studied the effect of particle distribution on the conductivity and shorting between connections. The particles studied had no interaction between them and randomly (Poissonianly) distributed over a two-dimensional space. They explored the statistical distribution of number of trapped particles on a given conducting pad area as well as studied the short circuit probability caused by chains of particles. However, in this work, the distribution of particles would not be concluded in advance. Instead, the calculations made were based on histograms of distribution properties on mono-layered particle images, as in figure 3.3 and 3.5.

For open circuit probability, it could be calculated directly from the histogram of the sub-region area fraction a. If consider an interconnect having less than a_o% area fraction covered by particle an open, the probability of this failure mode is then the total percentage of a no larger than a_o:

$$P_o = \frac{\sum_0^{a_o} N(a)}{\sum N(a)} \tag{3.6}$$

From cluster size histogram shown in figure 3.5, all information about size and number of particle clusters was provided, calculation of the probability of a cluster with size F_i short-circuiting a neighbor bump pair($F_i > g_b$) was carried out. Consider a sample with these properties, as shown in figure 3.6:

A : Area for bonding
w_b : Bump width
l_b : Bump length
g_b : Gap spacing between neighbor bumps

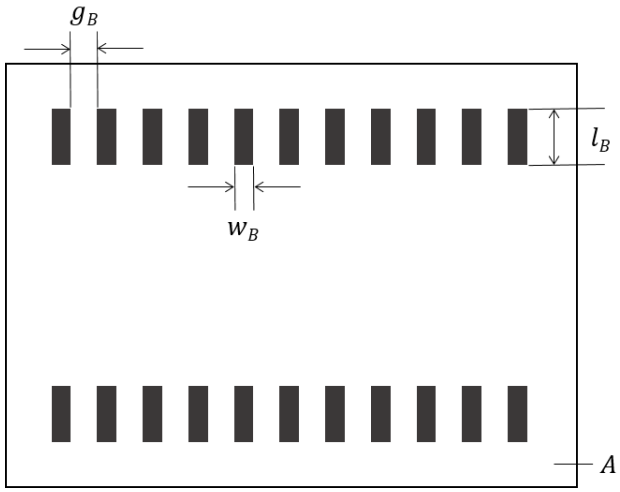

Figure 3.6: Dimension of Bumps and bonding area Shaded rectangles are bumps of w_b wide, l_b long and g_b distant from each other. Assume that these bumps are flat (very small height compare to particle diameter) and total area for bonding is A

Probability of the cluster fall into the gap space between one bump pair P_A equals the ratio of the gap space area over the total area of bonding:

$$P_A = \frac{l_b g_b}{A} \tag{3.7}$$

With the size F larger than bump gap g_b, probability of this cluster to lie in the short-circuit direction P_θ equals the area fraction of the circular sector of angle θ to the circle area, as shown in figure 3.7, i.e:

$$P_\theta = \frac{\theta}{2\pi} \tag{3.8}$$

$$\text{where} \qquad \theta = 2\arccos\left(\frac{g_b}{F}\right) \tag{3.9}$$

Probability of this cluster to short-circuit that bump pair in the sample:

$$P(F) = P_A P_\theta = \frac{n_g l_b g_b}{A}\frac{\theta}{2\pi} \tag{3.10}$$

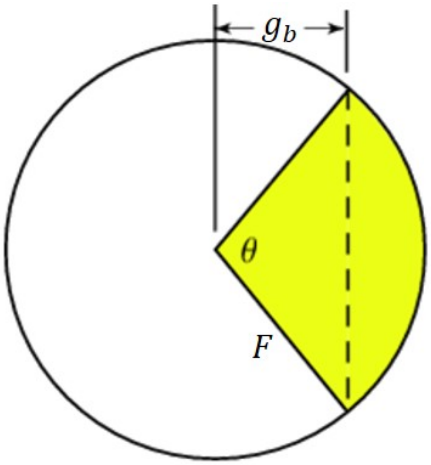

Figure 3.7: Area of a circular sector

If the ACA volume to be bonded contains n_F cluster with size larger than w_B, the total short-circuit rate of the sample equals total probability of short-circuiting caused by each cluster:

$$P_s = \sum_{i=1}^{i=n_F} P(F_i) = P_A \sum_{i=1}^{i=n_F} \frac{\theta_i}{2\pi} \tag{3.11}$$

P_s indicates the probability of the considered sample to have ONE bump pair shorted. Under such conditions as too long bump wall or too many large clusters, P_S can be larger than 100%, meaning that there can be more than two shorts within one bump pair.

P_s and P_o can also use to evaluate the quality of an ACA. However, they are not the general quantification parameters of distribution since additional information about the bonding sample (bump dimension and geometry) was needed, the size of particles and requirement of an interconnect. The relation of particle distribution parameters and failure rates will be estimated in next section.

3.4 Method validation

To evaluate the sensitivity of different distribution parameters as well as relation to the failure rate, images of four distinct distributions of same particle concentration were studied, as in Figure 3.8: (a) lattice-like, (b) random-like, (c) bad

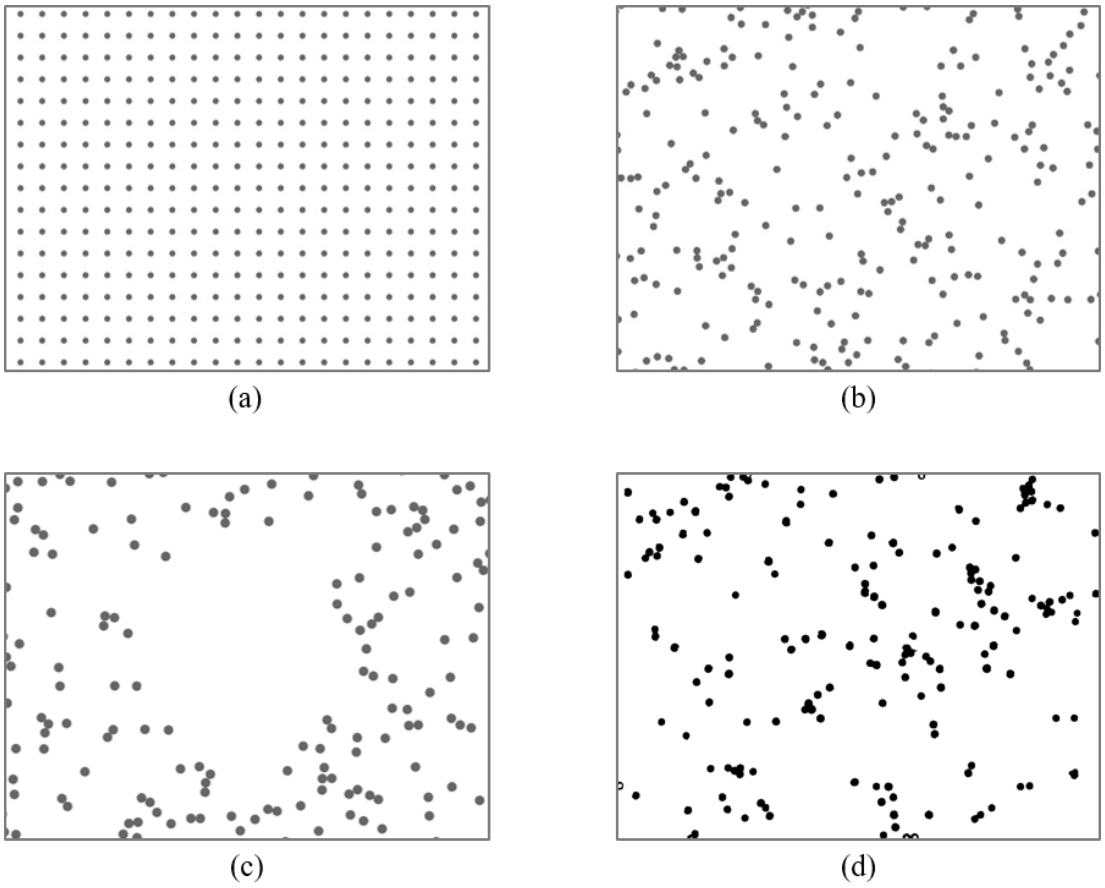

Figure 3.8: Examples of different particle distribution patterns-(a) Lattice-like distribution, (b) Random-like distribution, (c) Improper dispersion, (d) Improper clusterization

dispersion with unoccupied area and (d) apparent clusterization. Distribution parameters (clusterization C_k and dispersion D_k) as well as failure rate were analyzed. $k = 0.2$ was used for both C_k and D_k, and sample properties as detailed by Table 3.1 were used to calculate probability of failure. Obtained results are displayed by Table 3.2 and Table 3.3.

Table 3.1: Sample properties, $D_{0.2}$

Properties		Value
Bonding area (μ^2)	A	16×10^6
Bump length (μm)	l_b	100
Bump gap (μm)	g_b	15
Number of gap (μm)	n_g	96
Particle diameter (μm)	ϕ	5
Maximum area fraction of an open (%)	a_o	1.2

Table 3.2: Dispersion parameters, $D_{0.2}$

Example	Free-path spacing μ [ϕ]	Sub-region area fraction	Open-circuit rate
a	0.94	1.00	0
b	0.15	0.30	3.75
c	0.14	0.20	21.57
d	0.10	0.22	7.38

Table 3.3: Clusterization parameters

Example	$C_{0.2}$	Mean μ [ϕ]	Standard deviation σ [ϕ]	Short-circuit rate (%)
a	0.74	1.00	0.00	0
b	0.73	1.19	0.40	0.12
c	0.70	1.23	0.41	0.15
d	0.54	1.29	0.55	1.02

Table 3.2 shows dispersion parameters obtained from previous method, using free path spacing for calculation, and the modified method, using sub-region

area-fraction for calculation. The theoretical open-circuit rates P_o were also obtained. As displayed, two D_k values from two methods agreed well with each other for the first three samples (a) to (c). The open-circuit rate increase with the decrease D_k, meaning that the larger D_k is, the less probability of open-circuit failure occurrence. For lattice-like distribution (a) with particles evenly arranged through out the image, D_k for both cases was close to 1, and with uniform area fraction over the sample, open-circuit rate was apparently 0. These parameters of both methods dropped significantly for random-like distribution and decrease further for distribution with big unoccupied area in (c), and at the same time, P_o increased significantly.

However, when comparing (c) and (d), the two methods did not agree. First method indicated that (c) had better dispersion while second method claimed the contrary. In (c), apart from the unoccupied area, particles were dispersed reasonably well. On the other hand, particle spacing in (d) falls into a very wide range. However, using sub-region area fraction, the big empty area in (c) decreases D_k to less than that value of (d). P_o values indicate that (d) had lower open-circuit probability than (c). Therefore, D_k obtained by sub-region area fraction method agreed better with the failure rate predicted meaning that it was more suitable to evaluate the dispersion of particles in ACA bonding.

Three parameters representing the particle clustering were considered: clusterization parameters, mean and standard deviation of cluster sizes. The three parameters agreed well with each other in all cases, indicating that there was no clustering for (a), clustering to some extent in (b) and (c), and notable clusterization in (d). Short-circuit rate also increased with the decrease of these three parameters. The sensitivity of each parameter was, on the other hand, different. Comparison between the two cases (b) and (d), $C_{0.2}$ remarkably decreased by 25% while μ and σ increased 5% and 37.5% times respectively. Thus, this parameter $C_{0.2}$ was significantly more sensitive to the degree of clustering than mean value μ but less sensitive than standard deviation σ. However, since C_k was a percentage value, it can show how serious the clusterization of particle was, compared to the ideal case and worst case.

3.5 Pseudorandom distribution model

Distribution parameters, for how they are determined, are general values that does not depend on particle area fraction. Nevertheless, for particles that act in the same manner, clusterization and dispersion parameters will change with change of area fraction, similar to the Area disorder parameters discussed in [24]. Therefore, to have a better classification of particle distribution, a standard should be set. In this research, images with pseudorandom distribution of particle were generated and analyzed. The results can be used as a standard for evaluating a particle distribution, on whether it is better or worse than this pseudorandom distribution.

3.5.1 Algorithm of image generation

The term 'peusorandom' was rooted from the term 'peusorandom numbers' in Matlab. An image was generated first by setting particle diameter and particle area fraction of the image. Number of particles was then calculated and two set of uniform distributed pseudorandom numbers for x and y coordinates of particles's were created.

The next step was to separate overlapped particles. As shown in figure 3.9, when distance between two particles was smaller than particle's diameter, particles are separated by moving one particle to the side of the other particle in the same direction with the line that connect two particles' centers. This separation was to model the behavior of particles, which had no interaction, in real experiments. If assumed that the two overlap particles were in different height in three-dimensional space, when they were pushed vertically to each other to form one-layer, they would stay in direct contact and thus forming clusters. If simply removed one of the particle and replaced with new particle on different coordinates, then the clustering of particles would be much less than real situation.

The process was looped until all particles are separated. Images of different area fraction from 1% to 20%, with step of 0.1% and five images for each area fraction, were created and analyzed, using same calculation as described above to obtain clusterization parameters $C_{0.2}$ and dispersion parameters $D_{0.2}$ of pseudorandom distribution.

Figure 3.9: Separate of overlap particles

3.5.2 Pseudorandom distribution parameters

Figure 3.10, 3.11 and 3.12 show the modeling results of Pseudorandom distribution. For clusterization parameters depicted in figure 3.10, $C_{0.2}$ was stable around value 0.75 from 1% to 5% of area fraction. It later decreased linearly with the increase of area fraction. This behavior stemmed from the fact that the increase of area fraction would increase the mean cluster size , thus widened the range of calculation $0.8\mu_F - 1.2\mu_F$ but on the other hand, shifted this range further from 1 that made the probability density dropped dramatically. For small area fraction, where there were few particles, number of single particles was dominant, the widened range $0.8\mu_F - 1.2\mu_F$ led to slight increase of $C_{0.2}$. From area fraction greater than 5%, the exponential-like drop of cluster size was compensated by linear increase of calculation range, making the relation between $C_{0.2}$ and area fraction become nearly linear.

Mean cluster size on the other hand increased gradually and linearly with the increase of area fraction. This is understandable as more clusters presence meant more coordinator numbers, thus more overlapped particles and eventually, more and larger clusters formed.

The behavior of dispersion parameter was somewhat not straight forward to be interpreted. From 1% to 4%, there was an unusual change of $D_{0.2}$ but it could be explained by the histogram of pseudorandom distribution with area fraction of 2%, figure 3.13. It is clearly shown that sub-region area fraction a probability density was discrete for this low value of total area fraction. The peaks was corresponding to 0, 1 and 2 particles. When calculating $D_{0.2}$, if the mean area fraction μ_a fell into the middle of 2 peaks, the results would be low but if $\mu_a \simeq 1.7\%$ corresponded to second peak, D would increase significantly, displayed by the upsurge around 1.7% in figure 3.12. From 5% area fraction, $D_{0.2}$ increased linearly, since the histogram of a is now more continuous (figure 3.14). Unlike C_k parameter which had been modified to avoid this sudden transition due

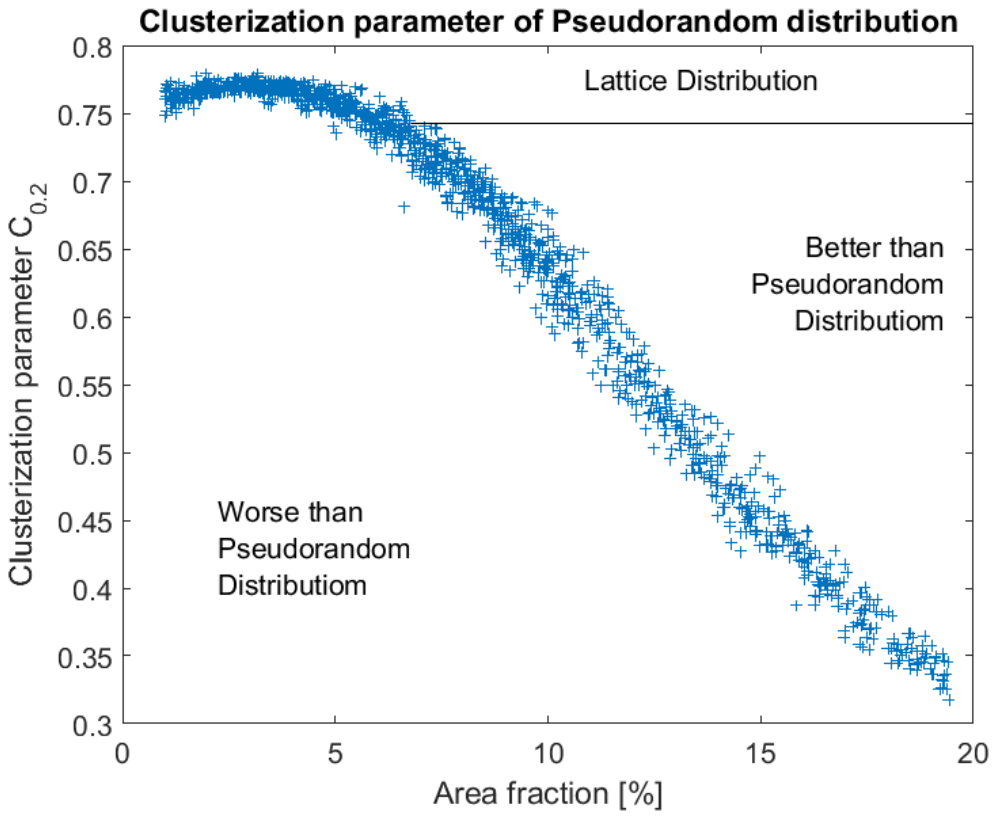

Figure 3.10: Clusterization parameter of Pseudorandom Distribution at different area fraction - $C_0.2$ is calculated by eq.3.5 or like in figure 3.5

to the non-continuity of values for calculating, D_k was left as it was. This was because sudden fall of C_k in the transition of μ_F from 1 to 2 then raise again when μ_F was near 2 couldn't reflect accurately the clusterization of particle (it should be higher when μ_F is smaller). However, the change in D_k on the other hand could give us an insight of what is the recommended value of total area fraction to have the stable dispersion behavior. Volume fraction for bonding real ACA should based on this recommendation as well, which was bonding area should be greater than 4%, correspond to 2.6%vol (if concentration of particles was the same before and after bonding).

According to this model, ACA should be made in a way that area fraction after bonding be in the range 5% to 10%, to avoid too much clusterization as well as too little particles. The model is also able to classify one distribution to be better or worse than this pseudorandom distribution. Evaluation on distribution of an ACA will therefore be more thoroughly.

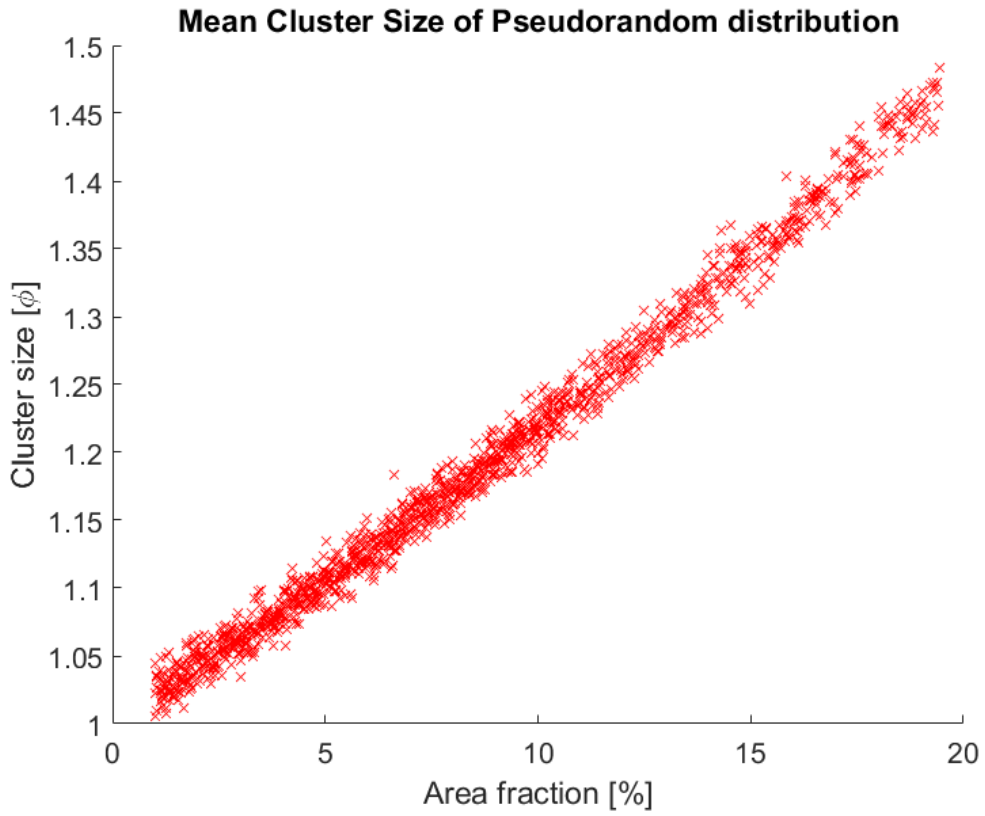

Figure 3.11: Mean cluster size of Pseudorandom Distribution at different area fraction

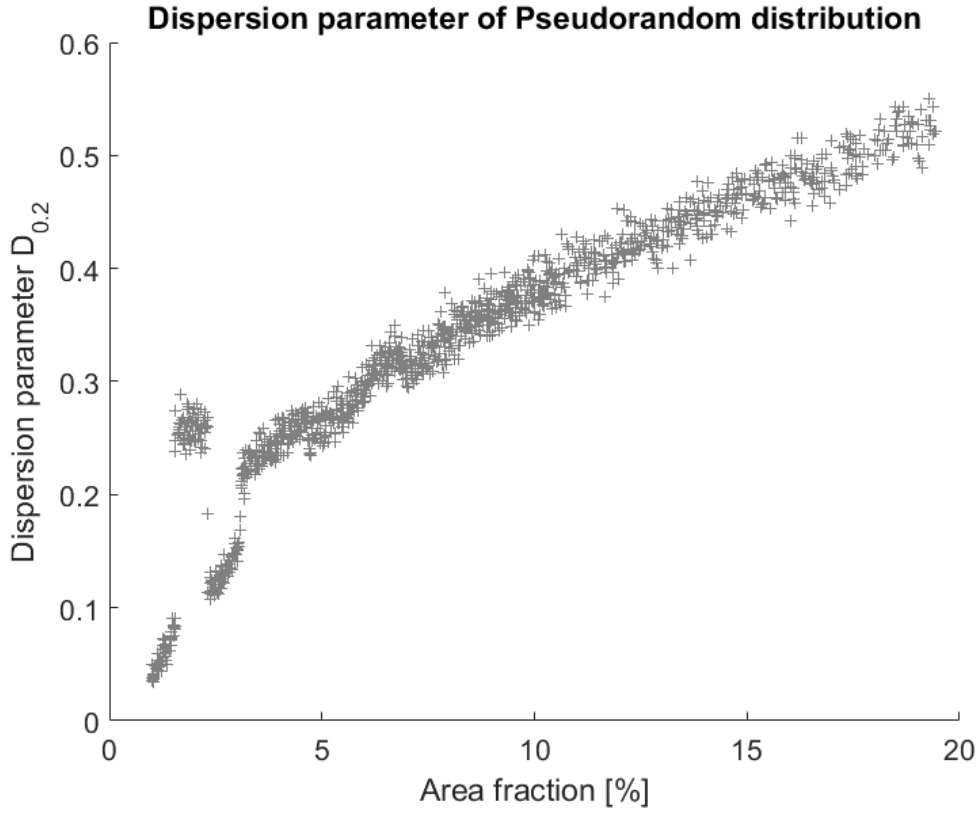

Figure 3.12: Dispersion parameter of Pseudorandom Distribution at different area fraction

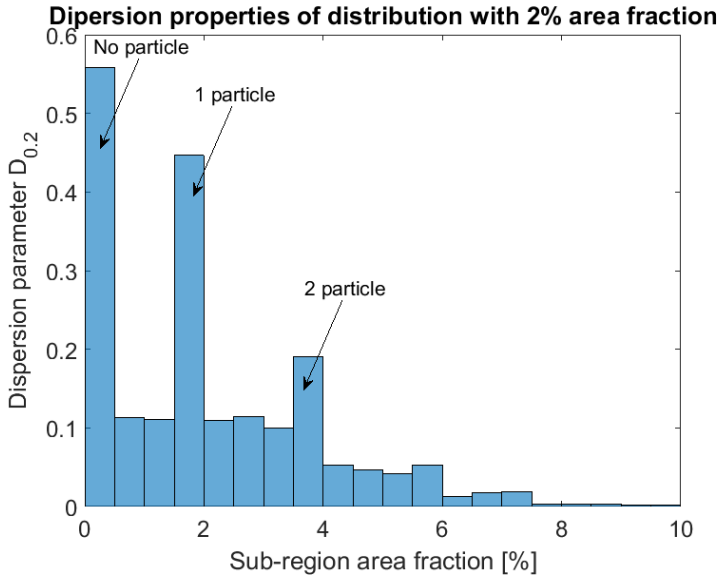

Figure 3.13: Sub-region area fraction histogram at area fraction of 2%

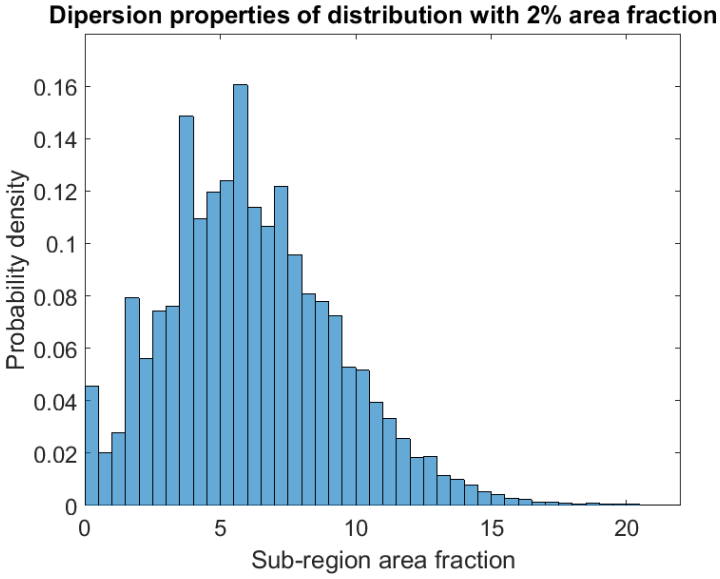

Figure 3.14: Sub-region area fraction histogram at area fraction of 6%

Chapter 4

Experimental

4.1 ACP preparation

To test the effects of spacers in flip-chip bonding, paste form of ACA was used. Preparation of ACP was carried out at Conpart AS, with epoxy system as adhesive matrix and MPS as conductive particles.

The metal coated polymer spheres used were supplied by Conpart AS, which were gold coated and mono-sized spheres of $5\mu m$ in diameter(Figure 4.1). The cores were made of highly crosslinked polymer allow the spheres to deform under compression while coated metallic layers (Ni/Au) made the particle conductive. Uncoated polymer spheres (UPSs) were used as gap spacers. They were made of the same core with MPSs with size of $3.3\mu m$ and used with larger amount in ACPs. Two types of UPS were used: origin UPS without any treatment and ethyl-acetate treated UPS.

Epoxy resin used was a low viscosity Bisphenol-F based resin to allow incorporation of high solid content. Hardener system was the combination of an amine adduct and dicyandiamide (DICY). Mixing ratio of these chemicals was in the way that after for a cure degree of 100%, reactive groups in epoxy as well as in hardener agents would all be consumed.

The treatment of UPS was to improve the incorporation of UPS into epoxy matrix. The process included mixing UPS with ethyl-acetate and epoxy resin. The mixture was then shaken manually for 30 seconds before drying in oven for 3 hours at 70℃to remove all ethyl-acetate.

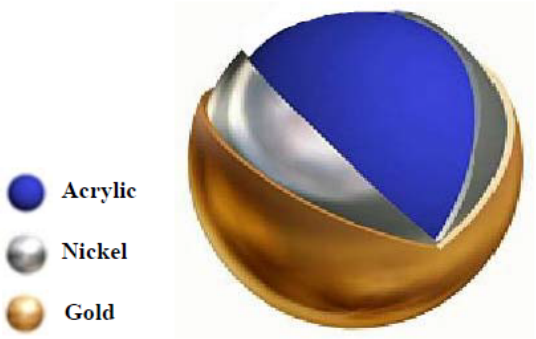

Figure 4.1:

Mixing process was carried out at Conpart AS using High speed mixer. The epoxy systems were first mixed under 2000rpm speed in 10 mins. Afterwards, MPS (and UPS if any) will be incorporating under 3500rpm in 2.5 mins.

4.2 Flip-chip bonding process

Flip-chip bonding process was carried out using a FinePlacer bonder. First step was picking up the chip/die by the bonding tool, in which a gimbal head was released and pressed to the chip on bonding surface. The force applied was high (40N) to ensure good co-planarity between bonding planes. Gimbal was then locked, and the chip was attach to the tool's head by vacuum. Substrate was then installed to the bonding table and alignment took place. ACP was then dispensed on the substrate, the tool head was lowered, temperature and pressure were applied.

Temperature profile of bonding process is shown in 4.2, in which 60℃was kept at the beginning then increased to 150℃with ramp rate of 3℃/s, this temperature (150°C) was kept at constant for 30s. Bonding force, which differed from samples to samples, was applied during bonding and released right after stopping heating.

Three types of bonding were made: non-patterned samples, samples for measuring insulation resistance and samples for measuring interconnects' resistance. Non-patterned samples were bonded for optical observation, each was made of a glass substrate of dimensions $20mm \times 20mm \times 100\mu m$ and a glass die of $4mm \times 4mm \times 500\mu m$. Short-circuit rate were evaluated by bonding same glass

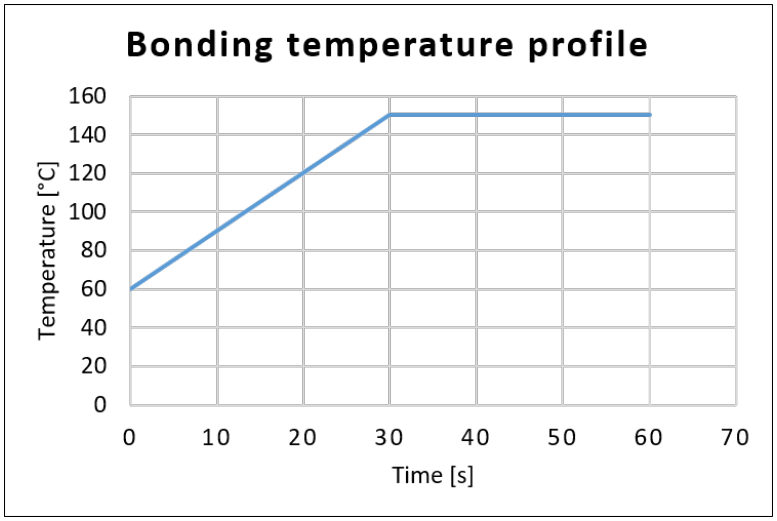

Figure 4.2: Bonding temperature profile

dies and substrates patterned for measuring insulation resistance (which were short-circuit components described in section 4.3.1). Samples for measuring interconnects' resistance were bonding of conductive glass die (ITO glass) of dimensions $4mm \times 4mm \times 500\mu m$ and resistance components (section 4.3.2). The ITO glass sheet resistance measured was $44 \pm 1\Omega/\square$.

4.3 Design of test devices

For electrical characterization of the ACAs, two types of substrate were designed for measuring interconnect resistance of individual bump and checking of short-circuit occurrence. These substrates were later bonded with smaller conductive or non-conductive glass dies, providing circuit and probing pads for electrical measurement. Configuration of measurement, described in detail by section 4.5.2, was considered carefully when designing.

All component designs were placed on the same wafer and fabricated at the same time, containing same metallic layers, i.e a copper wiring layer, a copper bump layer and a gold flash layer, deposited on an oxidized silicon wafer, see Figure 4.3. Copper was chosen as main metal because of its reasonable cost, high conductivity and ease of fabricating process. Wiring layer provided peripheral probing pads as well as circuits connecting bumps to these pads. The bumps

were designed high enough to prevent short-circuiting between wiring layer and the conductive glass. The top most gold flash prevented oxidation of bumps to ensure vertically electrical measurement of ACAs.

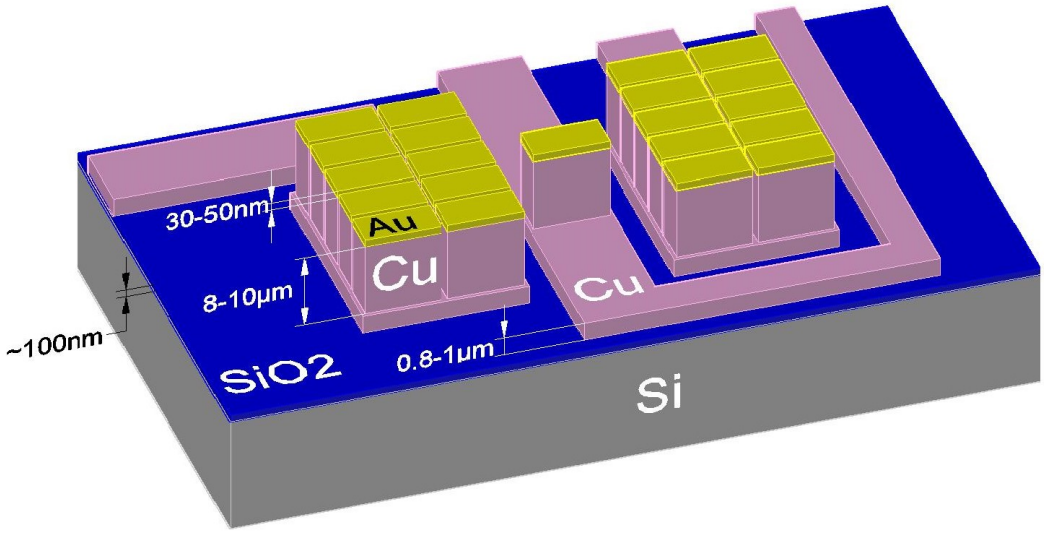

Figure 4.3: 3D illustration of a part of one component - Thin copper layer of about 1μm acted as wiring layer. Bumps were made of a 8-10μm thick copper layer with 30-50nm gold flash on top.

4.3.1 Short-circuit components

Short-circuit components made of comb-like structure consisting interleaved fingers were tailored for evaluate the rate of short-circuit occurrence in bonding. Three distinct designs were made, each consists of several pairs of combs with different numbers of fingers and width of gaps. Figure 4.4 depicts a specific design of this component type comprising 6 pairs of interleaved metallic combs. The 6mm high and 8mm wide substrate were bonded with smaller blank glass die of 4mm×4mm, revealing peripheral pads for probing. Two opposite pads were probe at the same time to measure the horizontal resistance between adjacent fingers of one comb pair. These designs were made in the way that short-circuit failure, even at small rate, still be detected in few measurements. Short-circuit

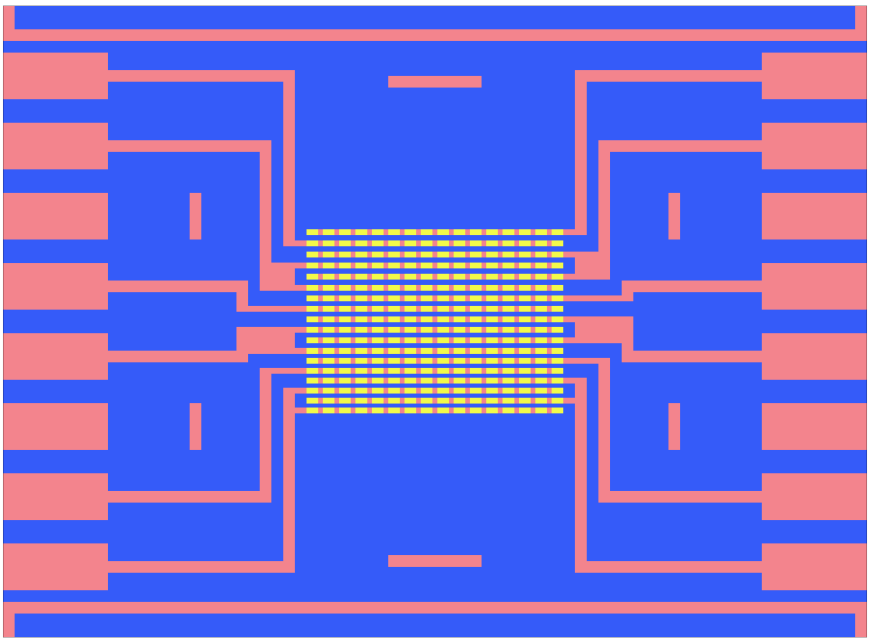

Figure 4.4: A component for short-circuit rate measurement - This design had widest gaps among 3 designs: 35, 40 and 45μm. Each gap size had 2 pairs of combs with 1 and 2 fingers respectively. Other two designs had 8 pairs of combs with gaps width of 10-12-14μm and 18-20-22μm respectively. Two-point probe on the pink sided rectangles was used to determine the insulation resistance between interleaved fingers.

was defined as when this resistance was less than 1GΩ. For the ease of fabrication, long fingers of width 50μm were divided to 16 lined bumps with dimensions of 100μm×50μm.

4.3.2 Resistance components

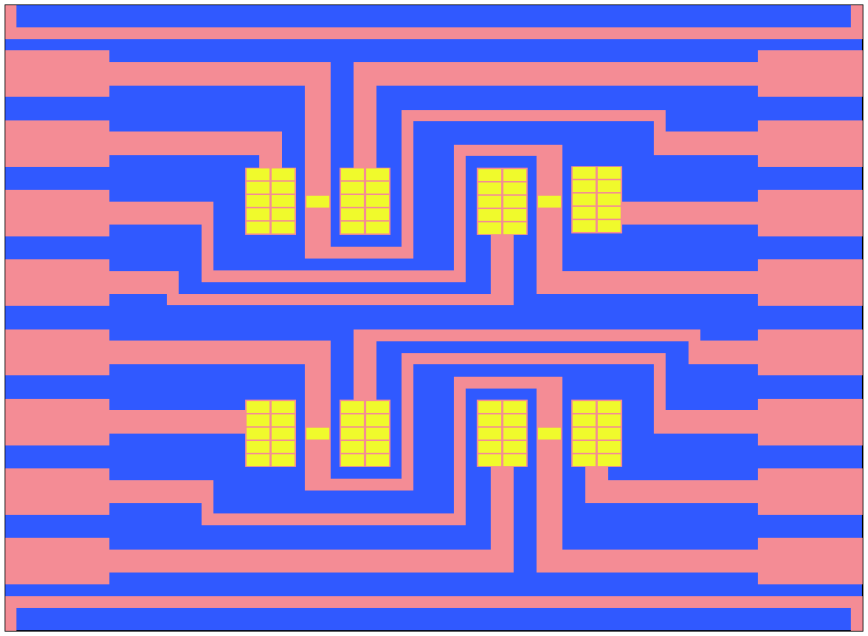

Figure 4.5: A component for interconnect resistance measurement - The design was make in the way that after bonding, contact resistance of the center small yellow bumps ($200\mu m \times 100\mu m$) can be probed with Kelvin measurement

Resistance structures, on the other hand, were used for measuring vertical resistance of ACPs, from the substrate bumps to the die. In each structure, resistance of 4 bumps at 4 positions were measured, to average out possible non-uniform co-planarity effects. For each interested bump, there were two sided bumps to configure Kelvin 4-point probes method. These sided bumps were design to be much larger than the interested bumps to ensure electrical connection from these bumps to bonded conductive glass so that the situation where an interested bump has connection but cannot be measure due to open at sided bumps would be avoided. However, since electroplating was chosen as deposition technique for these bumps, differences in bump dimensions might lead to uneven

plating of bumps. This will lead to open circuit at lower bumps. Therefore, the these large sided bumps were divided into small bumps with size equal to the interested bumps, see figure 4.5.

The design was made so that die patterning was not necessary, since all required wires and probe pads were on the substrates. The measurement configuration related to the designs is discussed in section 4.5.2.

4.4 Fabrication of test devices

4.4.1 Suggested fabrication process

A process was suggested for fabrication of testing devices. Seed layer for later electroplating was first deposited on a thermal oxidized silicon wafer. This step could be done either by sputtering or evaporating Copper. Deposition of a wiring layer then took place either with a lift-off process or an electroplating process. Bump layer was finally fabricated by electroplating 8-10 μm copper before sputtering or evaporating a thin gold flash on top. Two masks for wiring and bump layers was made according to the designs and suggested fabrication process.

4.4.2 Experiments

P-type silicon wafers were first thermal oxidized at 1000 - 1200℃ for 1h, forming a SiO_2 layer of 100 - 200nm. Adhesion of the seed layer to wafer was the key feature of the fabrication process since all layers were later added on this seed layer. Therefore, several techniques had been tried to figure out the suitable process for deposition of seed layer. First technique included sputtering a TiW (10/90) adhesion layer (20 or 100nm) in a vacuum chamber. Due to laboratory facility, opening chamber to replace sputtering target was unavoidable to sputter Cu (150-200nm) afterwards. The substrate temperature was around 20℃and sputtering rate was 3Å/s. Second technique was thermal-evaporating Cu directly on oxidized silicon wafer. Evaporation started at 10×10^{-6} bar with heating current of 85-90A to control depositing rate around 0.5-1 Å/s and stopped when Cu thickness reach 200nm.

After having seed layer, a photoresist layer (pr1) for lifting-off or electroplating wiring layer was casted on the wafers. Positive photoresist AZ-4562 of 4μm thick was photolithographed by spinning 4000rpm for 40s, soft-baking, UV-exposing for 65s then developing and hard-baking.

For lift-off process, a Cu layer of 1μm thick was sputtered or thermal-evaporated on pr1 then lifted-off by removing pr1 using acetone and remover. On the other hand, electroplating in a copper sulfate solution at room temperature with current density of $10mAcm^{-2}$ deposited 0.8-1.0μm Cu on other wafers, pr1 was removed afterwards.

Bump layer electroplating was patterned by second photolithography. This step was similar to previous photolithography, except the spin speed was changed to 1200rpm and exposing time was 100s, resulting pr2 layer of 11μm thick. Electroplating bump layer was carried out at same conditions as above but for longer time, plated 8-10μm Cu. 30-50nm gold flash was then evaporated at rate 0.5-1Å/s. Removing pr2 by acetone also lifted away Au outside bump areas. Final steps were etching seed layer by $Na_2S_2O_8$ 2% solution and dicing to single components.

4.4.3 Fabrication results

For seed layer deposition techniques, sputtered Cu, even with adhesion layer TiW of different thickness 20 and 100nm, did not adhered sufficiently to wafers. After immersing the wafer in copper sulphate solution for a long time to electroplate Cu, this seed layer began to peel off from the wafer (see figure 4.6). Evaporated Cu without any adhesion layer, on the other hand, remained still through the whole fabricating and dicing process.

Processes for depositing wiring layer, which were electroplate and lift-off methods, were both successful, as the layer adhered well to seed layer as well as attach the bump layer plated atop. However, due to the considerable complexity of the wiring layer, lift-off process took quite long time to fully remove all photoresist layer. Electroplating process was more suitable, with shorter processing time and lower cost.

In summary, feasible process for fabricating a designed wafer combined the chosen techniques for above steps, as described in figure 4.7. First, Cu was

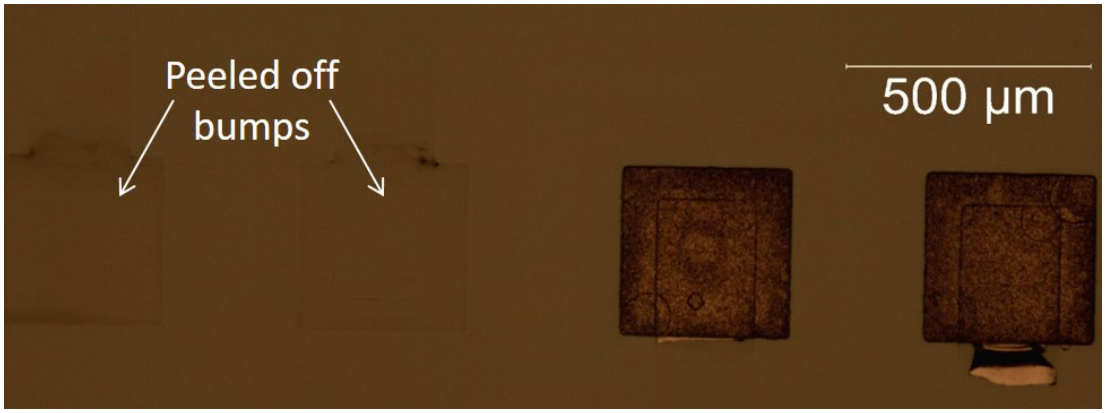

Figure 4.6: Peel off when using sputtered Copper

thermal-evaporated on an oxidized wafer forming a well adhered seed layer. Photolithography 1 deposits a $4\mu m$ photoresist (pr1) on the wafer for copper-electroplating of 1m wiring layer. After plating, pr1 was then removed prior to depositing a thick photoresist of 10-12m (pr2) that allows electroplating 8-10m Cu of bump layer. Gold flash was then evaporated on top of these electroplated copper bumps and pr2. Finally, Au on pr2 was lifted off, seed layer was etched away and the wafer was diced.

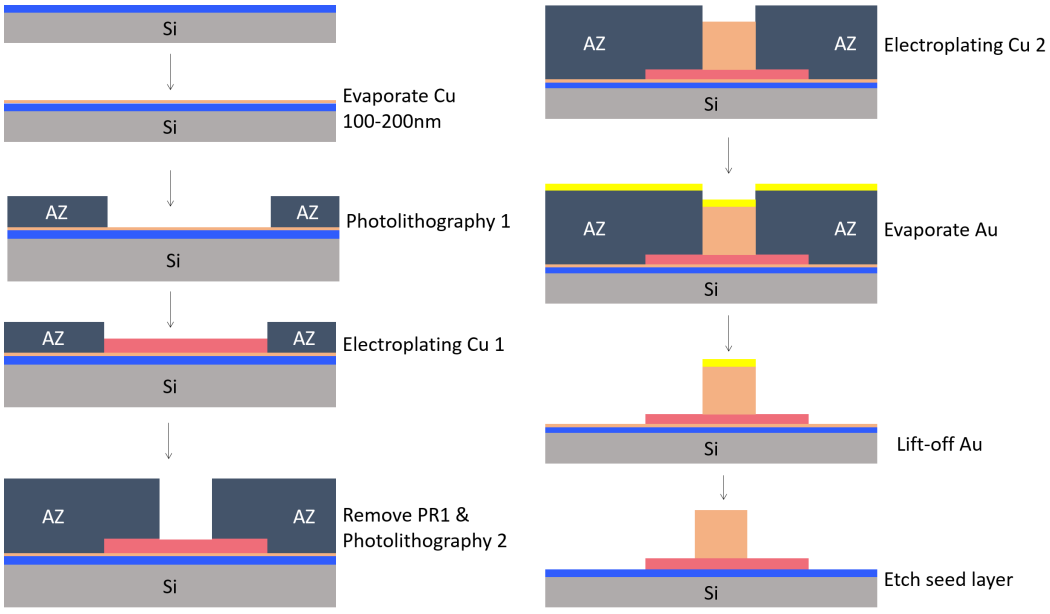

Figure 4.7: Final fabrication process

Fabricated components were inspected by white light interferometry, the results were shown by figure 4.8, 4.9 and Table 4.1. Fabrication results have shown that the fabricated samples were workable for electrical characterization of ACP. Fabrication results also proved that dividing large bumps in to small equaled bumps made bump height vary less, thus able to serve as testing components for further tests.

Table 4.1: Fabricated components' parameters

Parameters	Value range
Bump height (to track layer)	$8.5 - 10.0\mu m$
Track layer thickness	$0.8 - 1\mu m$
Bump height variation	100-300nm
Bump surface average roughness	100-200nm

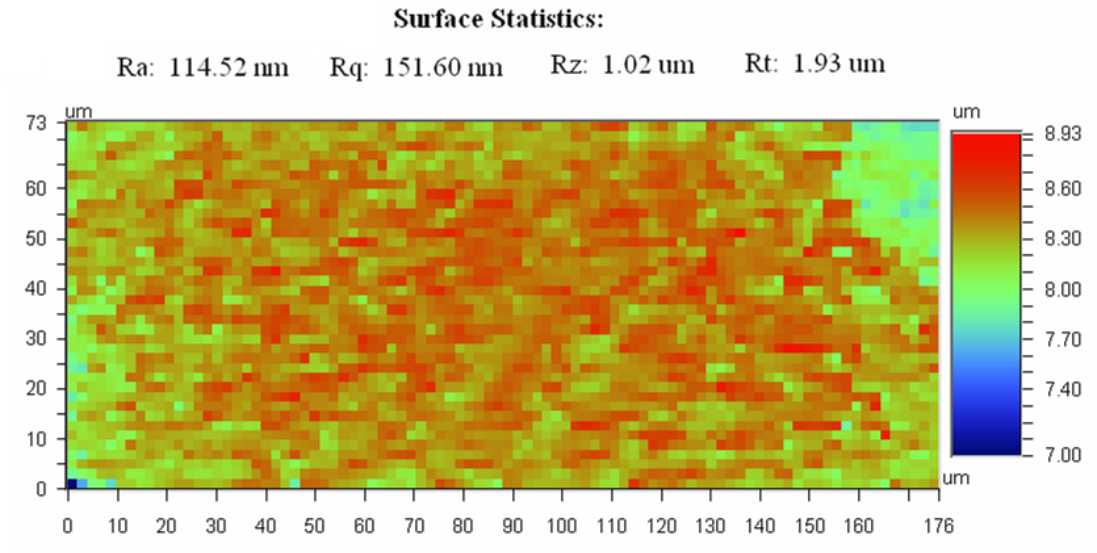

Figure 4.8: Surface statistic of a bump. - Roughness of bumps was acceptable for particle to have sufficient contact area to bump surface.

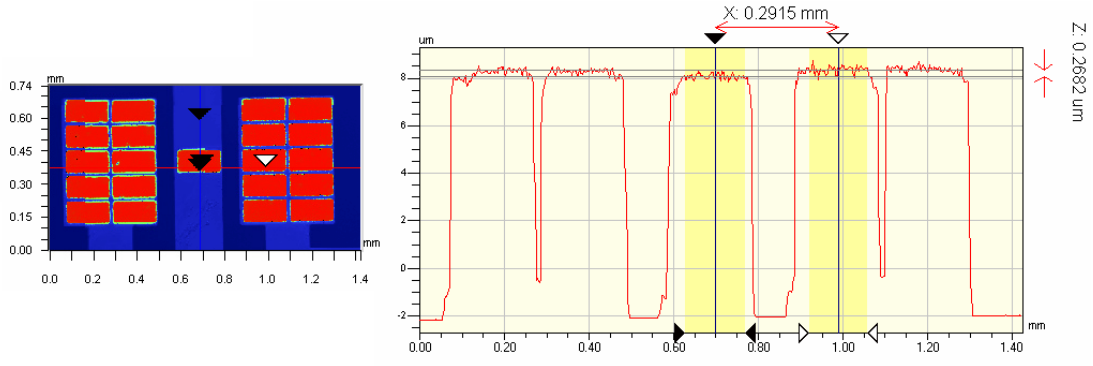

Figure 4.9: Bump height variation - The small centered bump was the one to be measured for resistance measurement. It should be at the same height with the two big bumps to have vertically electrical connection. With $5\mu m$ conductive particles, the bump variation of few hundreds nm was acceptable.

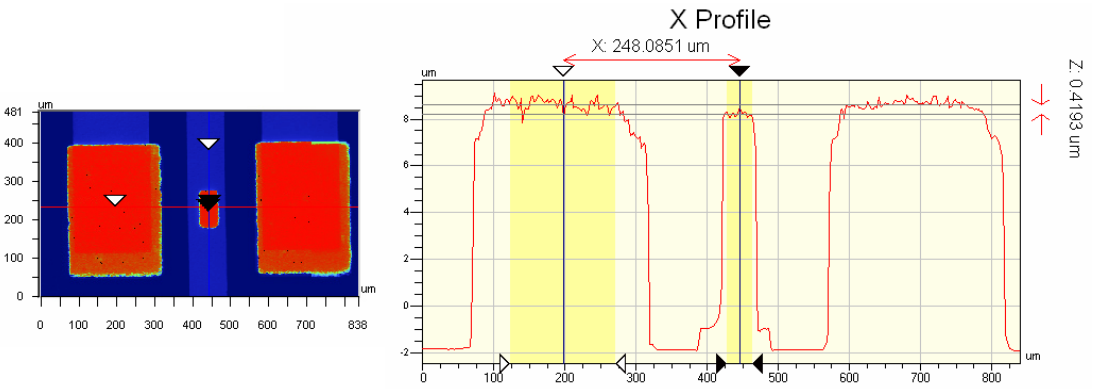

Figure 4.10: - Bump height variation for non-divided large bumps When the sided bumps were not divided, they become higher than the center bump. This may lead to open circuit of the center bump, which was the interested one. Therefore, this designs were not used for resistance measurement

4.5 Characterization methods

4.5.1 Distribution quantification procedure

Section 3.4 has proved the relation between failure probability and distribution parameters based on analytical calculation for two-dimensional cases. In real ACA applications, the method is not straight forward since ACA bonded in real sample indeed has approximately 3 layers of particles. Among these, one layer is on the bump surface to form interconnect, the other two are between bump walls. Therefore to apply the distribution analysis and failure rate prediction described in section 3.3 where images of adhesive with mono-layered particles are needed, some assumptions are of essence.

In this study, images of mono-layered particles were obtained by flip-chip bonding glass blank substrate and die. It was assumed that the distribution of particles on the bumps surface was similar to the mono-layer obtained with blank samples. Another assumption was that cluster sizes observed in blank samples will be similar but position in a three-dimensional space when bond in real samples. If these assumptions would be proven to be appropriate, this method can be used to quantify the distribution of particles as well as predict the electrical failure rate of the ACP before real bonding taking place.

The procedure for analyzing the flat (glass-glass) samples are shown in Figure 4.11. At 9 well defined positions on the bonded samples (a) images were captured using optical microscope (b). Each image was then processed (c) and analyzed using ImageJ software (d). Feret diameter of each cluster was recorded and further investigation was carried out on the binary images (c).

To apply the short-circuit prediction described in section 3.3, it was needed to modify 2D equations 3.11 and 3.6 to 3D. Now consider a 3D sample with these properties:

A : area for bonding
n_b : Number of bumps in the sample
w_b : Bump width
l_b : Bump length
h_b : Bump height
g_b : Gap spacing between neighbor bumps, $g_b \leq F_i$
H : Total thickness of the bond

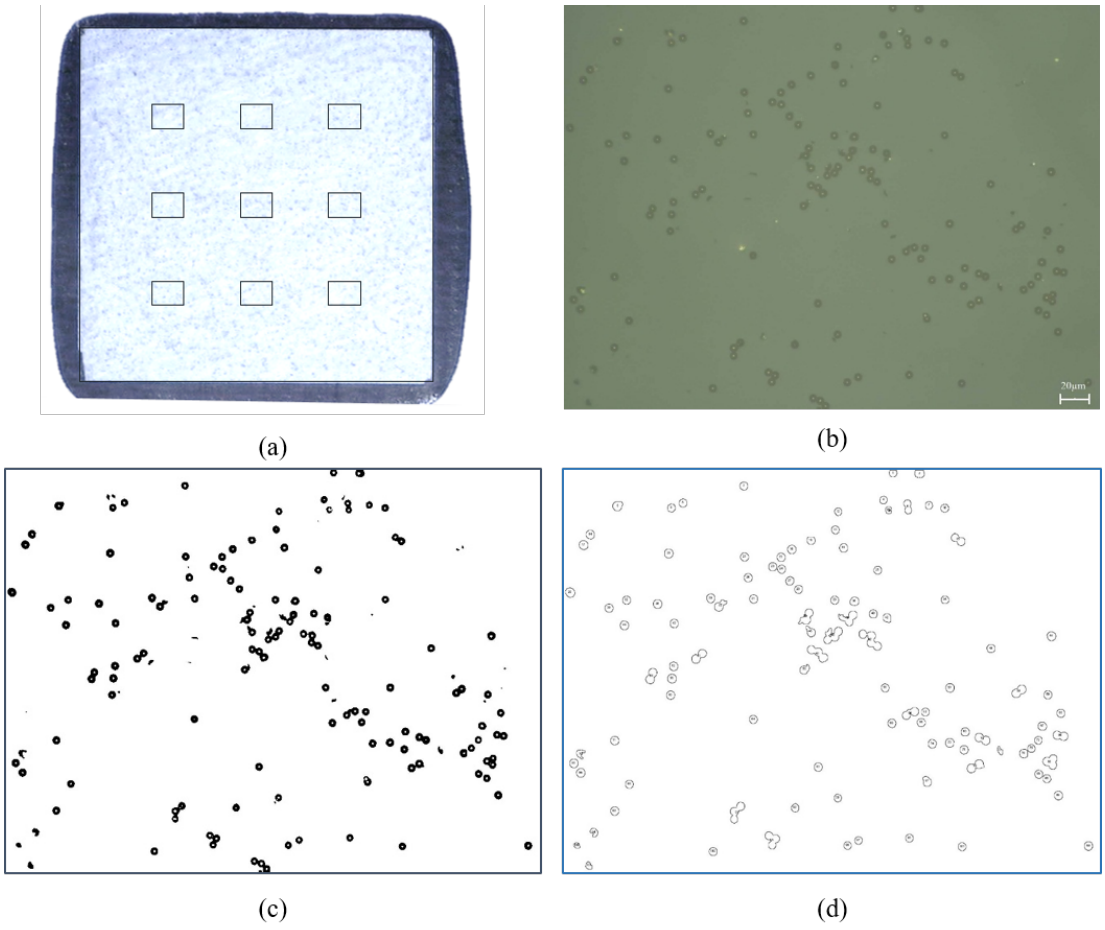

Figure 4.11: Procedure of obtaining, processing and analyzing images - ACA bond was made (a) and positions for taking microscope images were determined. These images (b) was then thresholded (c) and analyzed (d) using ImageJ freeware

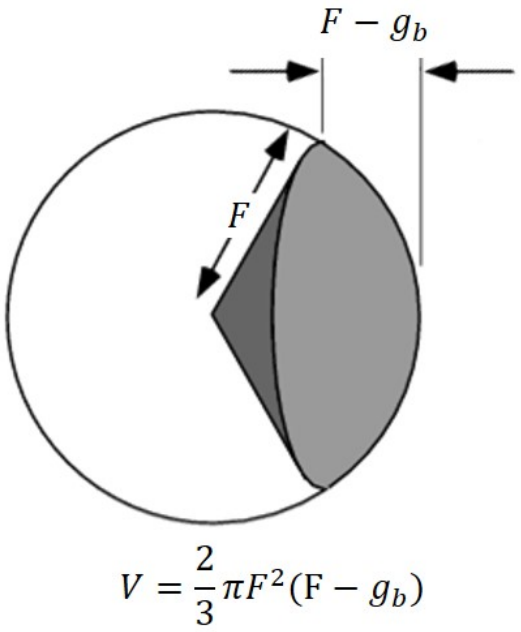

Figure 4.12: Volume of a spherical sector

P_A becomes P_V, which was the gap space volume fraction to the whole bonding volume.

$$P_V = \frac{l_b g_b h_b}{HA - n_b w_b l_b h_b} \tag{4.1}$$

P_θ of circular sector becomes spherical sector as in figure 4.12:

$$P_\theta = \frac{\frac{2}{3}\pi F_i^2(F_i - g_b)}{\frac{2}{3}\pi {F_i}^3} = 1 - \frac{g_b}{F_i} \tag{4.2}$$

Total probability becomes:

$$P_s = P_V \sum_{i=1}^{i=n_F} P_\theta(F_i) = P_V \sum_{i=1}^{i=n_F} (1 - \frac{w_b}{F_i}) \tag{4.3}$$

For checking the assumptions aforementioned, bumped substrates, designed and fabricated as describe in section 4.4, were bonded with blank non-conductive glass dies. Surface of bumps (figure 4.4) were analyzed to extract open circuit rate, while probing of side pads provides actual short-circuit rate (will be described in next section).

Particle covered area fraction of bumps a' were obtained following procedure described in figure 4.13. Actual particle-covered area fraction a' of bumps were

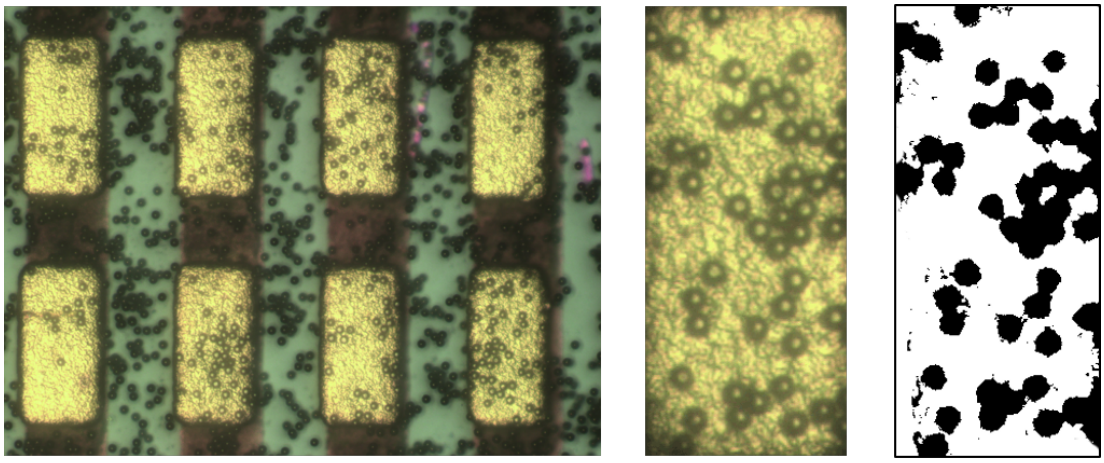

(a) (b) (c)

Figure 4.13: Optical images of bumps were taken (a). Surface of each bumps were isolated (b) and processed (c)

analyzed. A bump with less than 1.18% area covered (corresponding to 3 particles of 5μm in diameter cover a $50\mu m \times 100\mu m$ bump) were considered as an open interconnect. Open-circuit rate was then estimated.

4.5.2 Electrical measurement

Design of substrates for resistance measurement is shown in figure 4.5. These substrate were bonded with conductive glass ITO, provide both electrical and optical investigation. Kelvin set up was used for measuring the contact resistance of interested bump (center, small bump), as shown in figure 4.14. Equipment for measurement was Keithley 2100 instrument with 4 probing needles on a Probe Station PWS II.

Schematic of the set up are shown in figure 4.15, where:

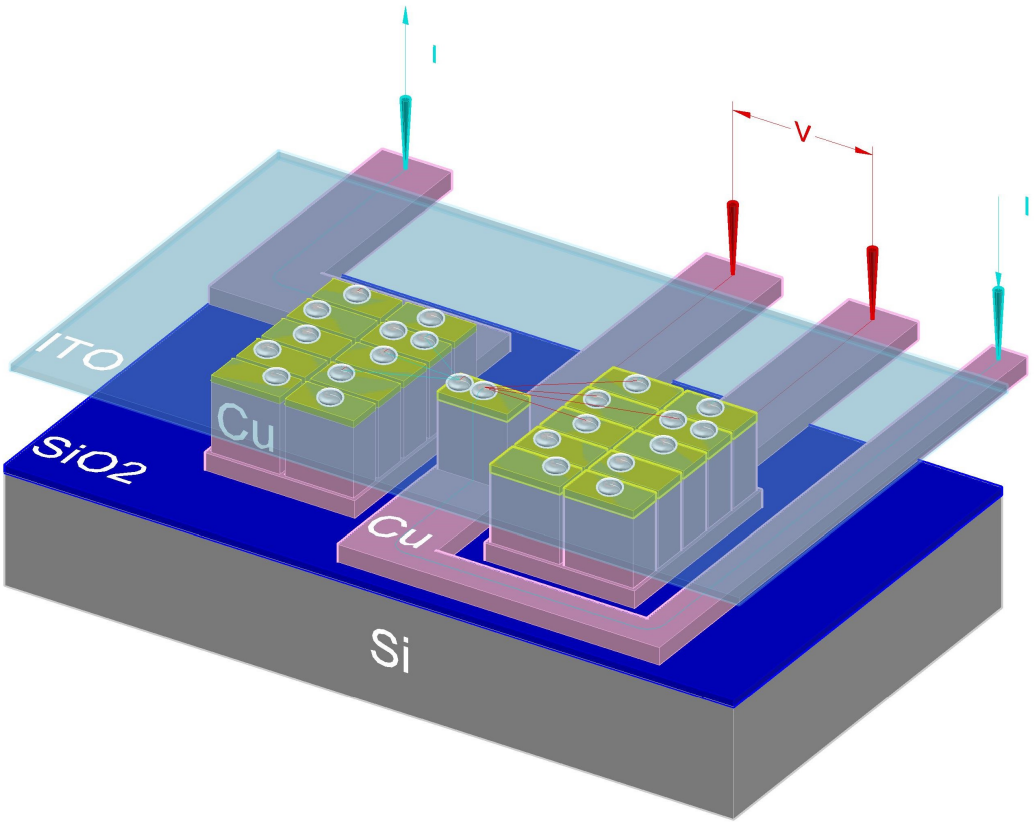

Figure 4.14: Four-point measurement set up

$R_{C,W}$: Resistance of probe contact and copper wire on the sample
R_B : Contact resistance of the ccenter bump to the ITO glass
R_{Sh} : Sheet resistance of ITO glass
R_{BB} : Contact resistance of the large bump to the ITO glass
I : Constant current from current source, $I = 1mA$
i : Small current to measure voltage, $i = 1nA$
V : Measured voltage

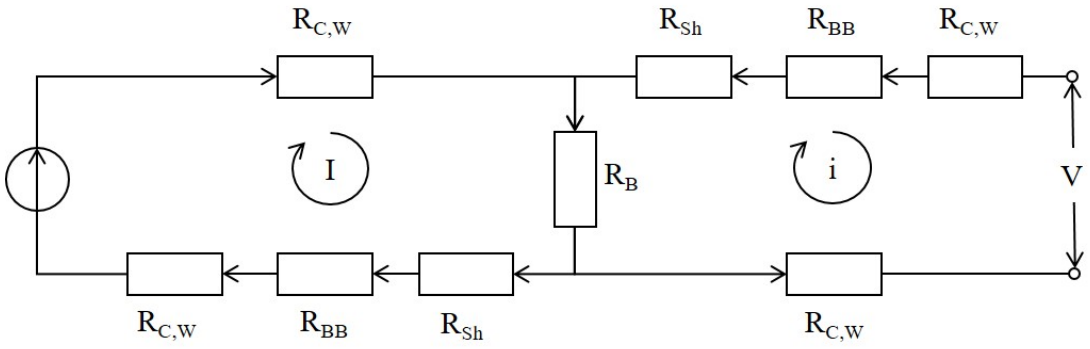

Figure 4.15: Schematic of the Kelvin measurement

According to the set up, measured resistance R_M is:

$$R_M = \frac{V}{I} = \frac{R_B(I+i)}{I} + \frac{i}{I}(R_{Sh} + R_{BB} + R_{C,W}) \approx R_B \text{ , since } i \ll I \qquad (4.4)$$

Therefore, the set up precisely measure the interested resistance.

Short-circuit detection was done my measuring the insulation resistance between neighbor bump rows. Substrates as depicted in figure 4.4 were bonded with non-conductive glass die. Measurement method was 2-point technique using same equipment. Current source was 1mA. Failure was define as when the 2-wire resistance measured was larger than 1GΩ. Two kinds of short-circuit components were used, one with spacing of 18-20-22μm and another with 35-40-45μm.

Chapter 5

Results

5.1 Incorporation of Spacers

Bonding of ACPs using original UPS and ethyl acetate treated UPS on blank glass dies and substrates were made to observe the bonding surface. Samples were bonded at 1.25MPa, with temperature profile described in section 4.2. Figure 5.2 shows the center of sample with original UPS and figure 5.3 shows four positions of the sample using treated UPS.

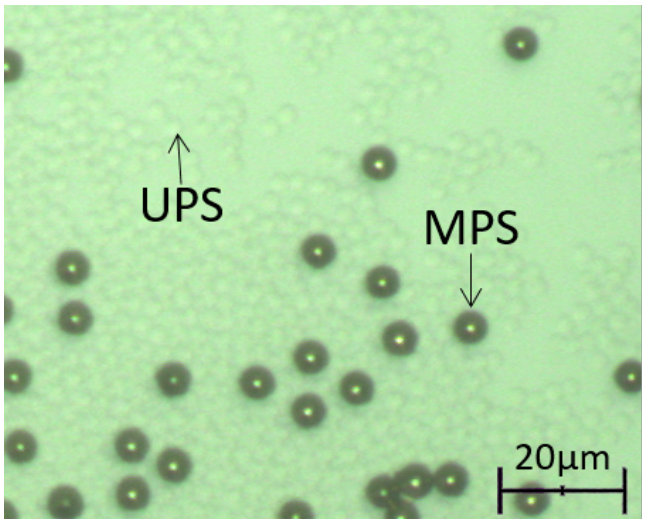

Figure 5.1: Particles in bonding surface - Small transparent particles are UPS and larger dark particles with shinny centers are MPS

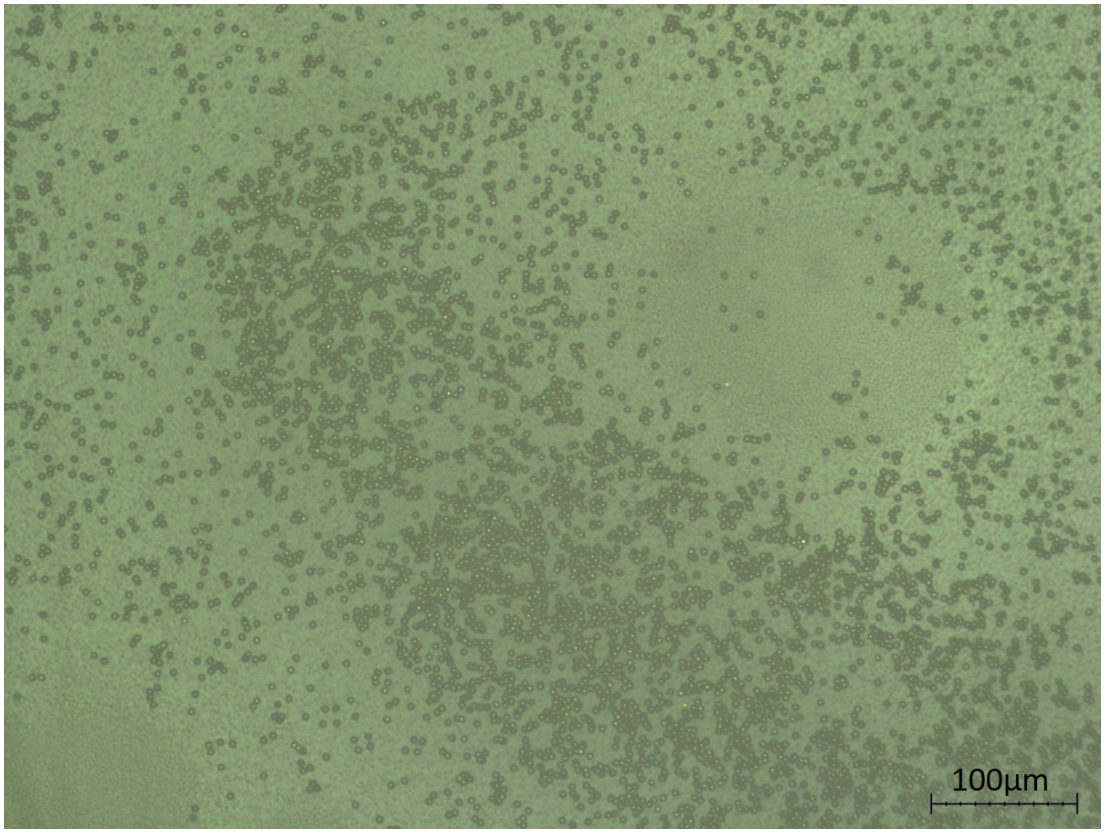

Figure 5.2: Bonding surface using ACP with UPS

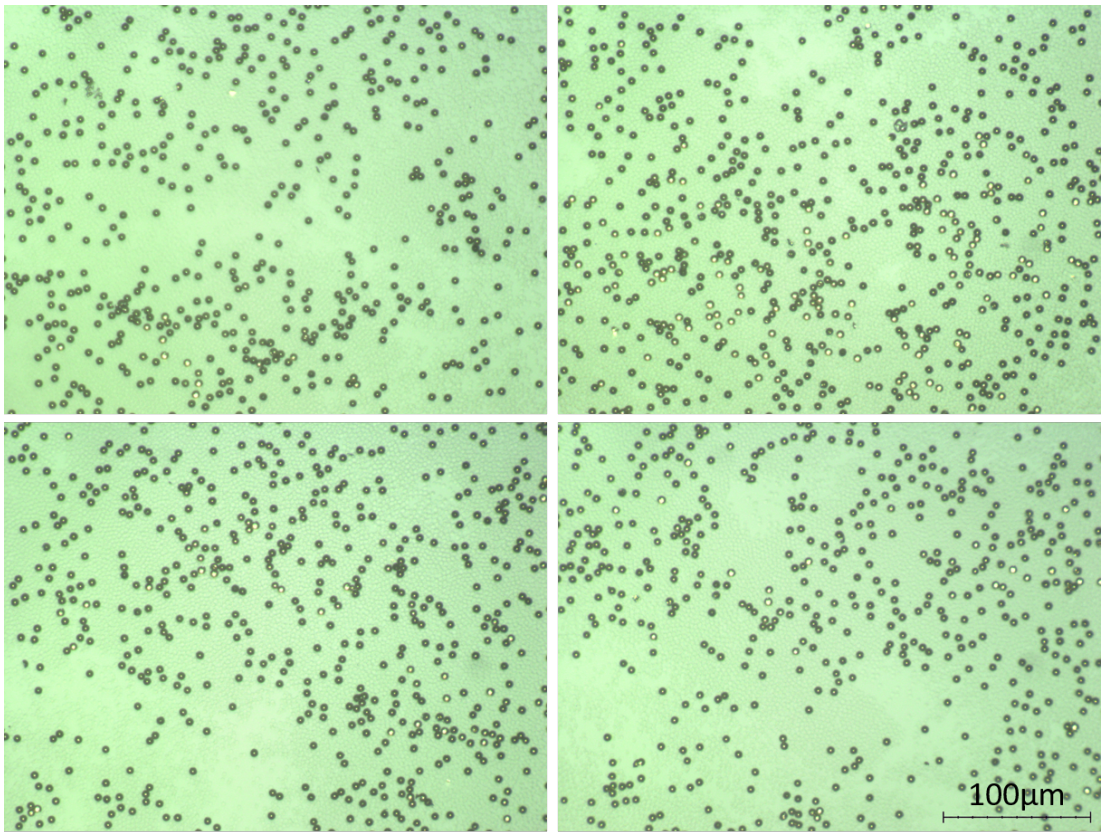

Figure 5.3: Bonding surface using ACP with Ethyl acetate treated UPS - Improvement of dispersion when the UPS are treated with Ethyl acetate is clearly observed.

5.2 Distribution and failure rate

Treated UPSs were chosen as spacers for further investigation. To verify the quantification method in ACA applications as well as study the effects of spacers, bonding of blank and patterned substrates were made using ACPs with and without spacers.

5.2.1 ACP without spacers

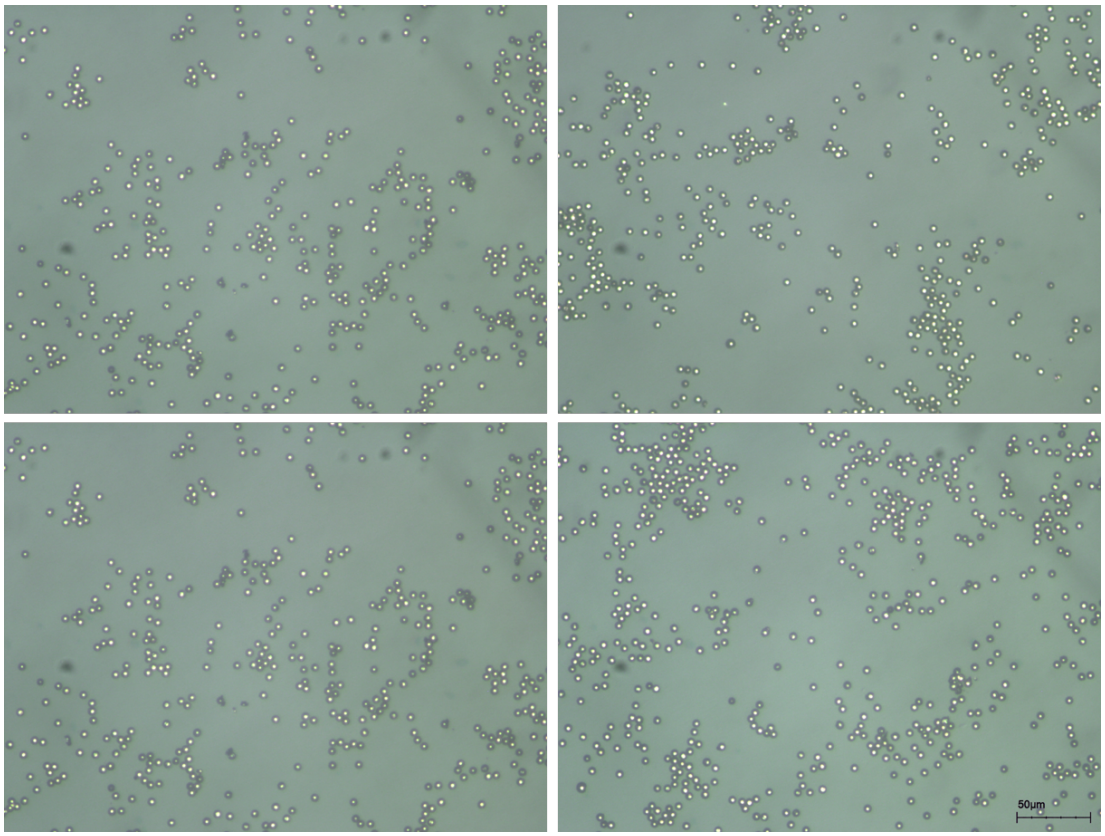

Figure 5.4: Bonding surface using ACP with 2%vol of MPS and no UPS

Bonding of ACPs without spacers were first made using different MPS volume fraction (1%vol, 2%vol and 3%vol) to determine a suitable MPS content for incorporating spacers. Bonding surface of ACP with 2%vol of MPS is shown in figure 5.4. Distribution parameters and predicted failure rate were obtained from non-patterned samples. For comparison, actual failure rates of patterned samples

are also included. Results are detailed by Table 5.1 and 5.2. That short-circuit rates were larger than 100% means more than one short could occur within a bump, since the calculated bumps were extremely long.

Table 5.1: Clusterization of MPS without spacers

Properties		1%vol	2%vol	3%vol
Blank samples	$\mu_F[\mu m]$	7.47	8.19	8.08
	$C_{0.2}$	0.39	0.25	0.17
	Short-circuit rate predicted	333.76% for $l_B = 5.6mm$, $g_B = 18\mu m$	1137.92% for $l_B = 100\mu m$, $g_B = 20\mu m$	39.52% for $l_B = 100\mu m$, $g_B = 40\mu m$
Patterned samples	Short-circuit rate measured	21% for $l_B = 5.6mm$, $g_B = 18\mu m$	42% for $l_B = 5.6mm$, $g_B = 20\mu m$; 3% for $l_B = 0.8mm$, $g_B = 18\mu m$;	22% for $l_B = 1.6mm$, $g_B = 40\mu m$

Table 5.2: Dispersion of MPS without spacers

Properties		1%vol	2%vol	3%vol
Blank samples	Mean area fraction μ_a [%]	7.05	13.15	14.36
	$D_{0.2}$	0.20	0.24	0.26
	Open-circuit rate predicted [%]	8.47	2.74	2.03
Patterned samples	Mean area fraction $\mu_{a'}$ [%]	3.07	5.69	9.17
	Open-circuit rate measured [%]	4.86	2.26	0.17

Histograms in figures 5.5, 5.6 and 5.7 show the sub-region particle area fraction in comparison with actual particle area fraction on bump surface.

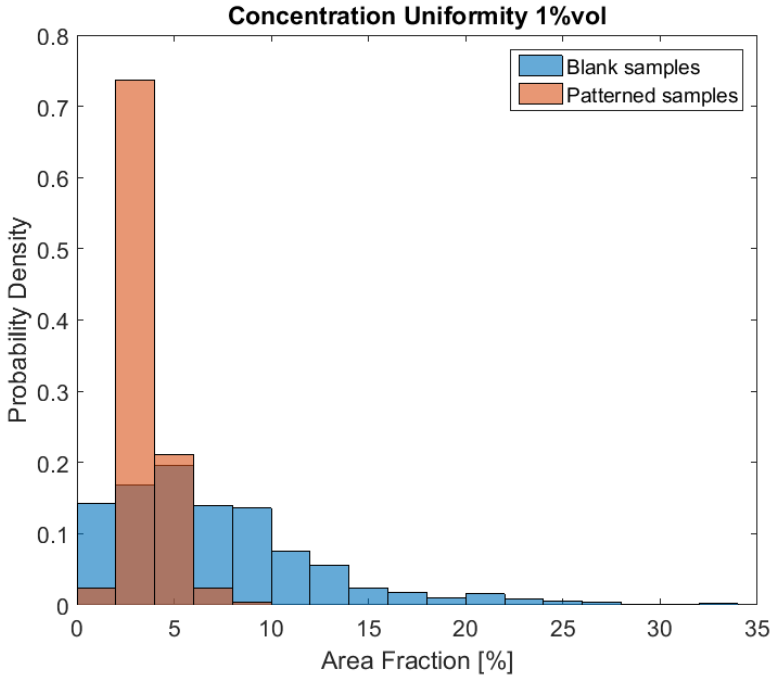

Figure 5.5: Histogram of area fraction for ACP with 1%vol MPS

5.2.2 Spacer effects on particle distribution

From previous results, it can seen that ACPs with $3vol\%$ results a higher area fraction than theoretical calculation (in which area fraction of same sample should be 1.5 times of volume fraction), for both blank and patterned samples. This resulted in a low rate of open-circuiting but on the other hand high risk of short-circuiting was obvious. On the contrary, if only $1vol\%$ of MPS were mixed into ACP, possibility of lacking particles for conduction was significant. Therefore, the volume fractions chosen were 1.5 and $2vol\%$ of MPS into 2 ACPs repectively, together with $20vol\%$ of spacers for both adhesive.

Table 5.3 details the clusterization parameters for ACPs with spacer, in comparison with ACPs without spacers. No short-circuit failure was detected down to spacing $g_b = 18\mu m$ and total bump length $l_b = 32.8mm$ for ACP with 2%vol MPS

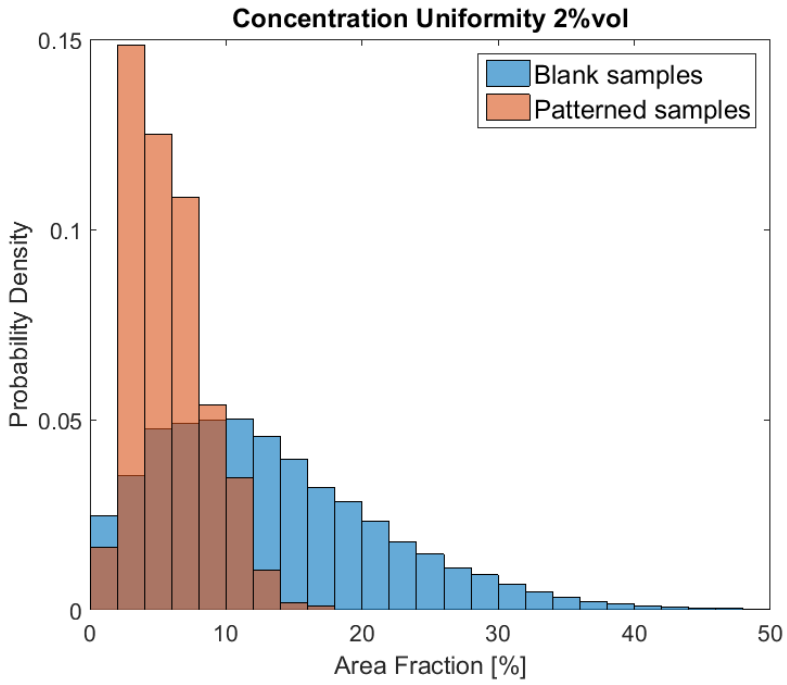

Figure 5.6: Histogram of area fraction for ACP with 2%vol MPS

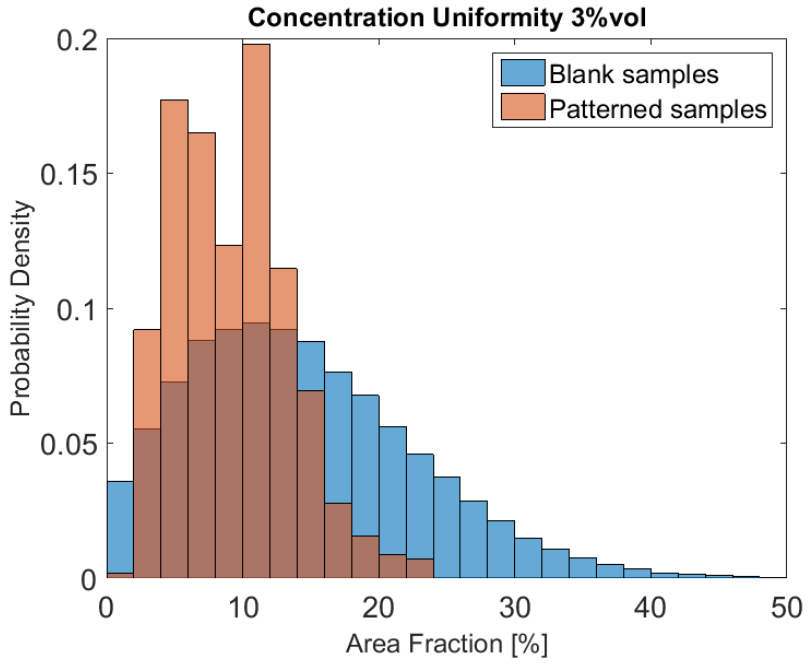

Figure 5.7: Histogram of area fraction for ACP with 3%vol MPS

and 20%vol spacers. Cluster size histograms of APCs with and without spacers are plotted in figure 5.8 Table 5.4 shows dispersion parameters of the two ACPs.

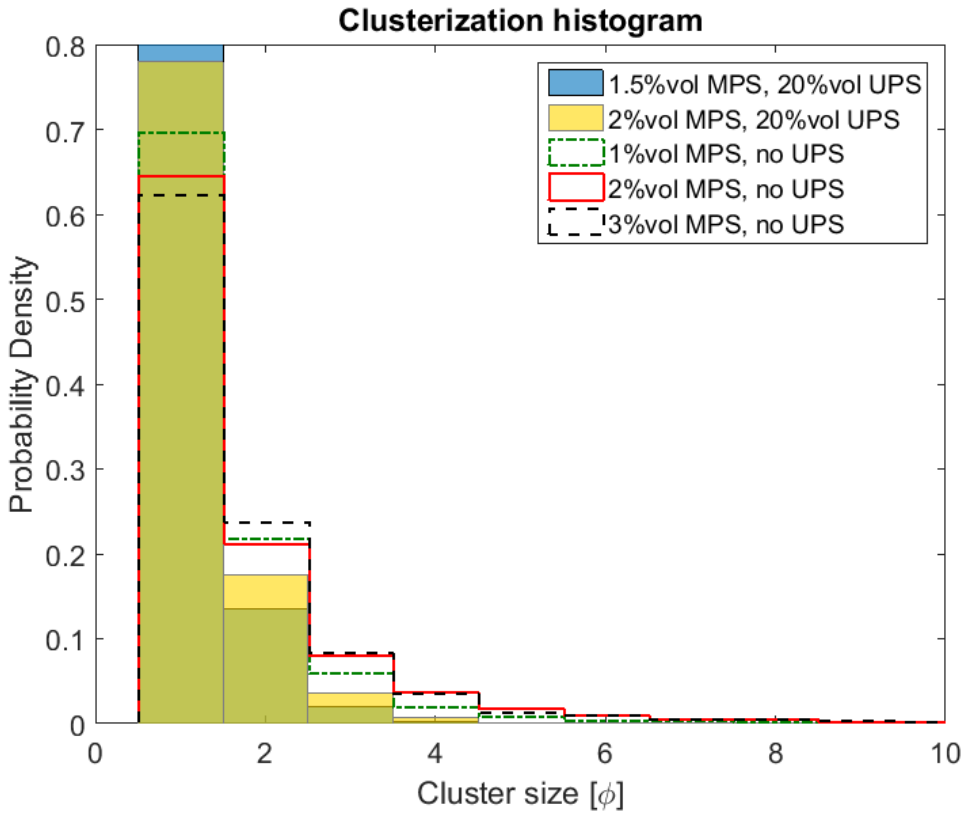

Figure 5.8: Histograms of cluster size of ACP with and without spacers

Figures 5.9 shows histograms of sample using ACP with spacers, with comparison of area fraction on blank samples and area fraction on bump area of patterned samples. All the distribution parameters of bonded non-patterned samples are shown in figure 5.10 and 5.11.

5.3 Electrical resistance and deformation

Bonding of ACPs with and without spacer were made under different bonding force 10, 20 and 30N, correspond to 6, 12 and 18MPa on bump area respectively. Figure 5.12 shows the resistance of these samples with respect to corresponding

Table 5.3: Clusterization of MPS spacers

Properties	1%vol MPS, no spacers	2%vol MPS, no spacers	1.5%vol MPS, 20%vol spacers	2%vol MPS, 20%vol spacers
Mean cluster size $\mu_F[\mu m]$	7.47	8.19	6.09	6.26
$C_{0.2}$	0.39	0.25	0.70	0.58
Predicted short-circuit rate for $l_B = 100\mu m$, $g_B = 18\mu m$ [%]			0.56	2.46

Table 5.4: Dispersion of MPS with spacers

Properties		2%vol MPS, no spacers	2%vol MPS, 20%vol spacers
Blank samples	Mean area fraction μ_a [%]	13.15	13.11
	$D_{0.2}$	0.24	0.37
	Open-circuit rate predicted [%]	2.74	0.53
Patterned samples	Mean area fraction $\mu_{a'}$ [%]	5.69	7.13
	Open-circuit rate measured [%]	2.26	5.03

force. Quantitative evaluation of particle deformation on the bump surface is shown in figure 5.13.

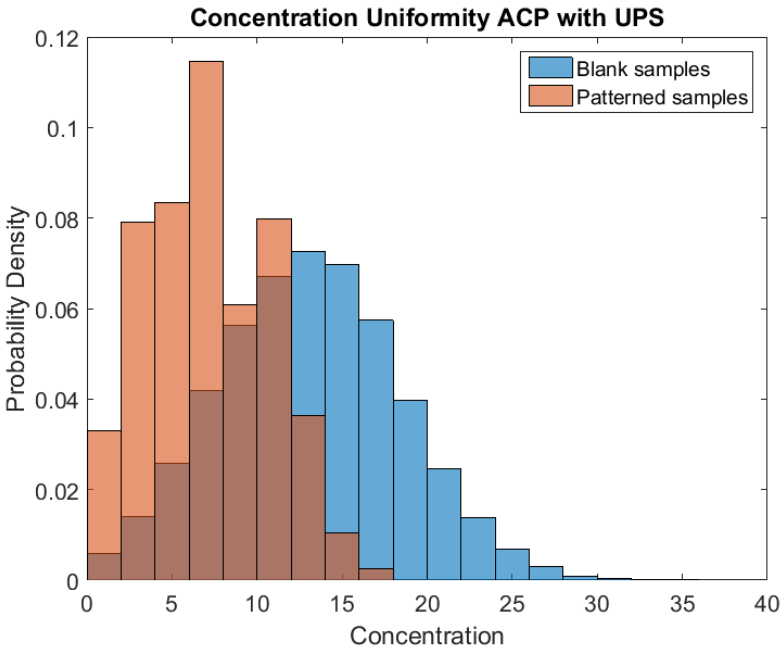

Figure 5.9: Histogram of area fraction for ACP with 2%vol MPS, 20%vol UPS

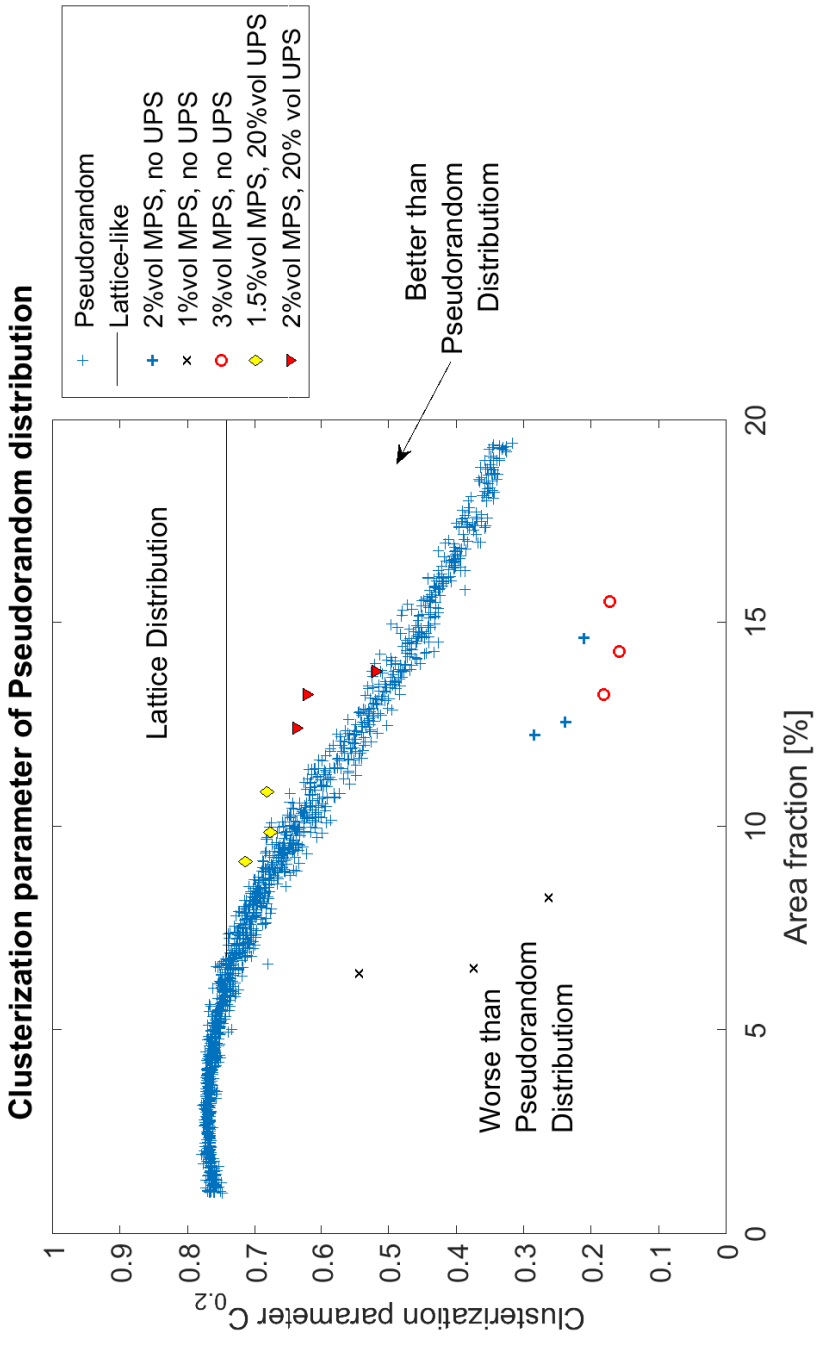

Figure 5.10: Clusterization parameters of all blank samples

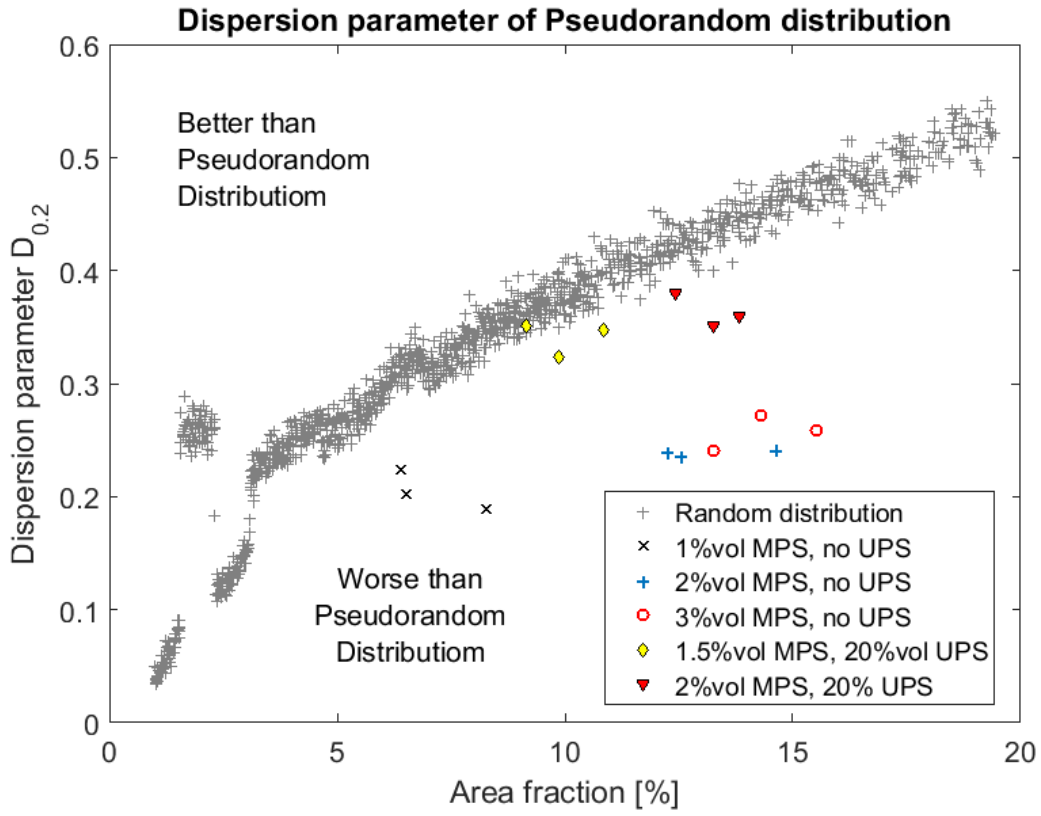

Figure 5.11: Clusterization parameters of all blank samples

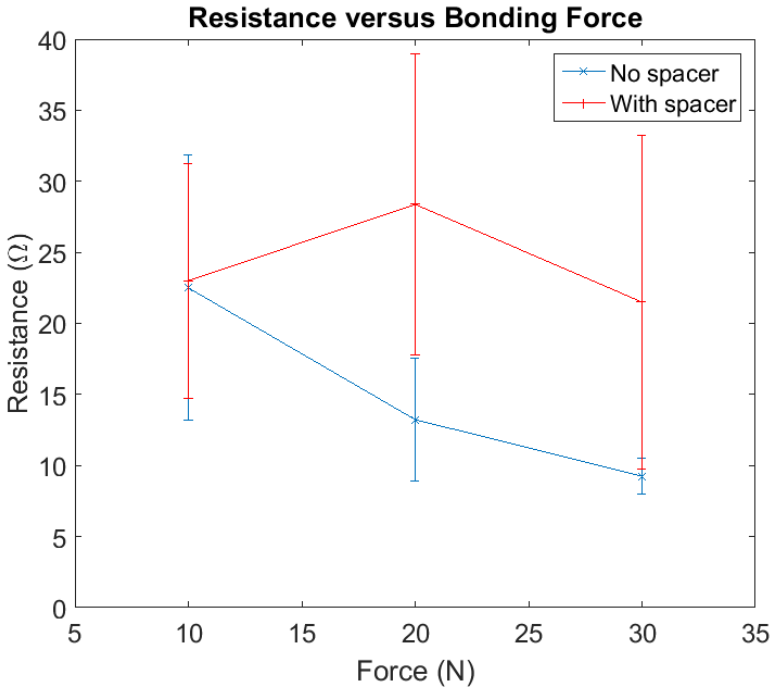

Figure 5.12: Resistance of 2 ACPs under diffenct bonding force Resisteance of ACP bonding comparing ACP with and without spacers for different bonding force

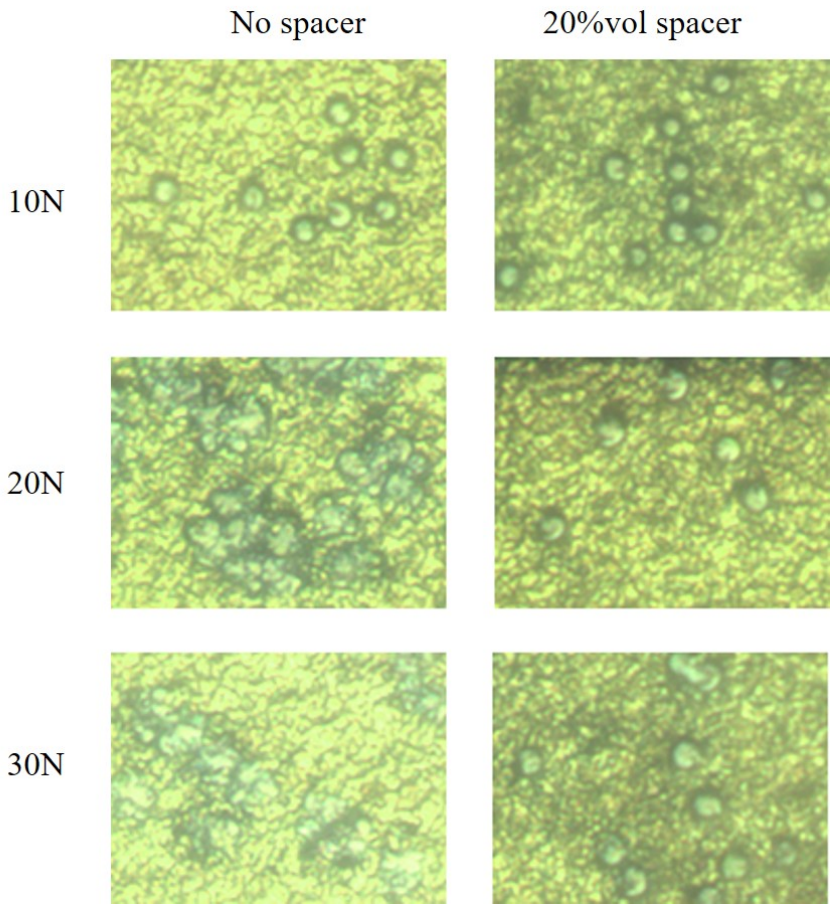

Figure 5.13: Resistance of 2 ACPs under different bonding force It can be seen that the use of spacer particles delays the fracture of the conductive particles

Chapter 6

Discussion

6.1 Incorporation of UPS to epoxy matrix

As can be seen from figure 5.2, the incorporation of original UPS spacers into epoxy system was poor. Separation of UPS was significant with massive clusters. This phenomenon stem from the fact that wetting of epoxy on to acrylic surface of UPS was poor. From wetting theory discussed in section 2.4, epoxy with surface tension $\gamma_{LV} \sim 42mJ/m^2$ [23] cannot wet well acrylic surface with critical surface tension $\gamma_C \sim 39mJ/m^2$ [31].

Large clumps of UPS also lead to agglomeration of MPS around them. For ACA bonding, this adhesive was inapplicable since the probability of open-circuit in UPS cluster region was apparent while agglomeration of MPS would easily cause short-circuit.

To improve the wetting of epoxy to acrylic UPS, treatment of UPS should be done. Figure 5.3 shows the distinct improvement of dispersing UPS into epoxy system after treating UPS. Although there were still some non-uniformity of UPS area in the bonding plane, treated UPS particles no longer agglomerates into big clusters. These were consequences of treating UPS with ethyl acetate. Mixing epoxy resin and ethyl acetate (with lower surface tension $\gamma_{LV} \sim 24mJ/m^2$ [32] and lower viscosity than epoxy) promote the wetting on UPS particles' surface. Particles were separated, coated with mixture of epoxy and ethyl acetate. After removing the ethyl acetate with drying, UPS particles remain separated and a

layer of epoxy still covers the particles. Distribution of MPS was significantly better compared to that of samples with original UPS.

6.2 Effects of spacers on distribution and failure rate

Table 5.1 shows that for clusterization properties of ACPs, C_k values of all adhesives were low, indicating a distribution that was far from random-like distribution. Smaller values was seen in higher concentration of MPS. Short-circuit rates predicted were safe.

Comparison of particle dispersion properties between blank and patterned samples shows some differences but there was a consistence between three ACPs. Mean values of area fraction in blank glass samples were higher than that in patterned samples. Bondings was carried out using flip-chip bonder, in which, blank dies were bonded on top of the patterned substrate. This means that highest places on the substrates were bump surfaces, this lead to less particle were trapped on bumps. However, the statistical distribution of area fraction covered by particles on bumps a' were better than a (sub-region area fraction) of blank samples. $D_0.2$ values of a and a' indicate that particles dispersion on bumps area was more uniform than on blank samples. Histograms plot in figures 5.5, 5.6 and 5.7 also present a narrower span of a' values. Open-circuit rate predicted by blank samples were also higher than patterned samples, indicating that prediction from blank samples were safe.

As displayed in figure 5.8, for both cases (with and without UPS), there was more large particles in ACPs with higher amount of MPS. Possible explanation for this outcome was that the higher amount of MPSs an ACP contains, the higher probability of these particles to form large clusters. This phenomenon gets more serious if the interaction between particles are stronger than that between particles and adhesive matrix. More particles means more area for interaction, thus more clusters are formed. Compared between ACPs with and without spacers, the effect of spacers on clusterization of particle was remarkable. Clusters sizes of ACPs with spacers have narrower span and higher probability density in small size. Analyzed and summarized results of these histograms are presented

by table 5.4. Not only the mean sizes noticeably decrease but the clusterization parameters also increase to close to that value of random-like distribution. Short circuit rates predicted also drop sharply. These results show that clusterization parameters change in good consistency with cluster size histograms and predicted short-circuit values. This once again proves the accuracy of this parameters on evaluating ACPs' quality, with regards to short-circuit failure mode. Low predicted short-circuit rate was also evidenced by measurement on patterned component, in which even contains higher content of MPS (2%vol compared to 1%vol), ACP with UPS still has better results with regards to short-circuit rate than ACP without UPS. Effects of UPS on clustering properties of MPS in epoxy matrix was possibly because UPS particles can act as barriers which prevent MPS impact and interaction.

Figure 5.10 once again confirmed the improvement in clusterization of ACP with spacers compared to ACP without spacers. The clusterization parameters became even higher than that of pseudorandom distribution, meaning that cluster sizes of theses samples distributed in a narrower range, therefore more uniform (in cluster size) and less large clusters. While on the contrary, clusterization parameters of ACP without spacers were far below pseudorandom's values, indicating serious clusterization in these samples, evidenced by short-circuit rate measured.

Dispersion parameters displayed in 5.4 also show an improvement when using spacer, as $D_0.2$ raises 54% and open-circuit prediction decreased by 4 times. As shown in figure 6.1, area fraction values in bonding with spacers disperse in a narrower span than that in bonding without spacers, mode value was higher as well. Figure 5.11 also shows that dispersion parameters of ACP with UPS were superior to that of ACP without UPS, and nearly equaled to pseudorandom values.

When bonded with patterned components, ACP with spacers traps overall more particles (higher mean area fraction) and, as shown in figure 6.2, has higher mode value (value with highest probability density). This was in consistency with blank samples. However, the actual open rate of bonding using ACP with spacers was 2 times higher than that of ACP with no spacers and 10 times higher than prediction on blank samples. This can be explained by the fact that UPS has lower weight density than MPS, therefore, there was still some vertical separation in ACP into UPS-rich regions and MPS-rich regions. In non-patterned

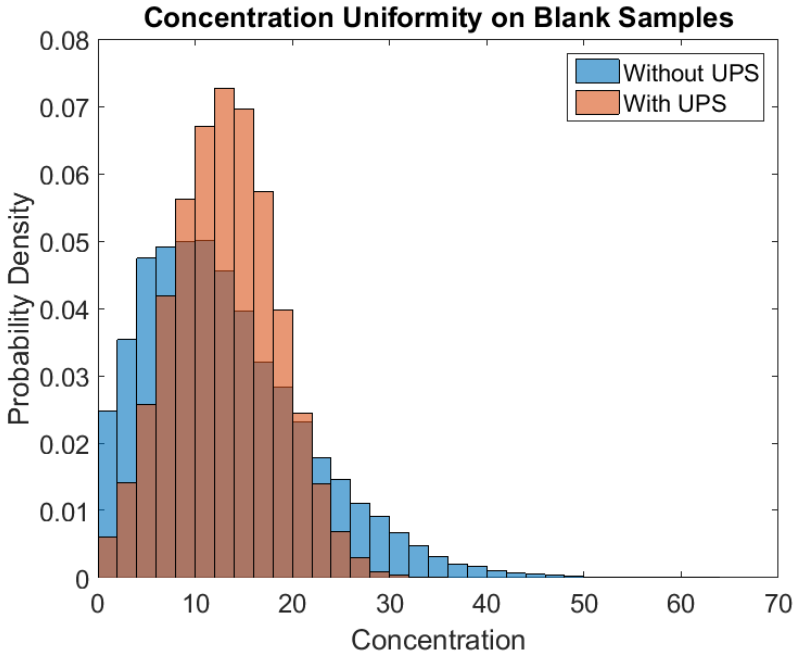

Figure 6.1: Comparison of area fraction of non-patterned samples with and without spacers

samples, bondings were in mono layer, these regions will merge and no difference in concentration be detected. On the other hand, in patterned samples, bondings were in three-dimension and the flow of paste was complex, the higher viscosity of ACP with spacers (due to higher solid concentration) allows more particles to be trapped in overall, but the difference in particle concentration, especially with some regions have low MPS content, leads to higher open-circuit rate (more bumps have less than three particles) than ACP without spacers.

The high open-circuit rate might hinder the electrical properties of ACP, but so far, the performance of spacer with regards to distribution of conductive particles was promising. Volume fraction of MPS can be increased further than these amounts to improve conduction properties and decrease open-circuit probability, since the short-circuit rate was still low.

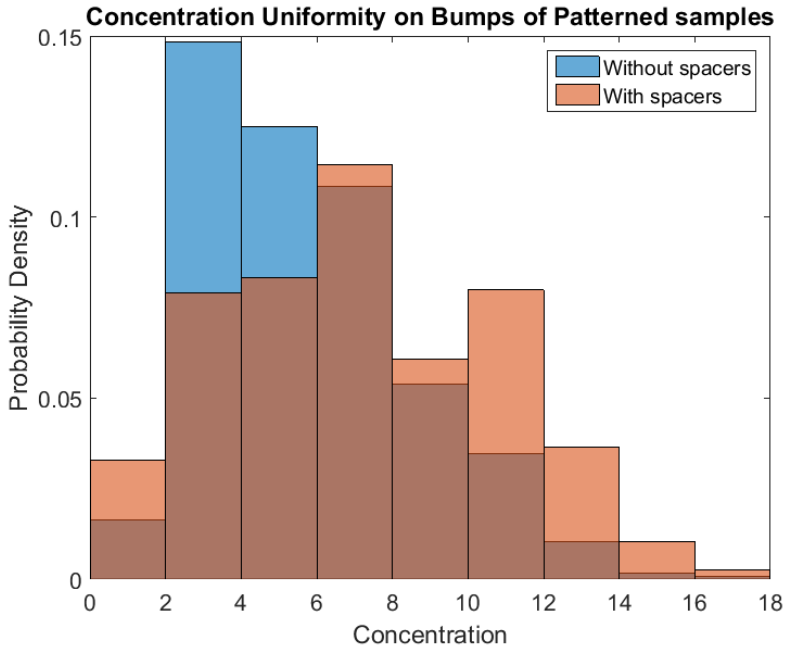

Figure 6.2: Comparison of area fraction of patterned samples with and without spacers

6.3 Effects of spacers on electrical resistance and deformation

Results shown in figure 5.12 indicate that the resistance of ACP contain spacers did not change with force, and was similar to resistance of ACP without spacers at 10N. Resistance of ACP without spacers resistance, on the contrary, reduced gradually with force. Compared with figure 5.13, the resistance changed in consistency with particle deformation. Starting from 10N, deformation and resistance of the 2 ACPs were similar. Increasing force from 10N to 30N, in samples with the presence of spacer, deformation of particle was qualitatively unchanged and resistance values were similar. Under same conditions, on sample without spacer, bonding force had a remarkable influence that particles were crushed when bonding force was larger than or equal to 20N, and resistance decreased with increase of force. In this test, the high resistivity of ITO coated glass used were the explanation for the high resistance of the contact.

With the obtained results, it was evidenced that the incorporation of spacers does prevent larger conductive particles from crushing inside the interconnect. These crushed particles, although were able to yield lower resistance, can cause some reliability problems. Preventing particle crushing and control the deformation of conductive particles may not reduce the resistance but make it more consistent and governable. This can also allow a wider window of applying force in real industrial process. Furthermore, the size of spacers used in the study has not been optimized to govern the best deformation of conductive particles thus the electrical resistance obtained was not minimized.

Chapter 7

Conclusion

Deformation and distribution of conductive particles play key roles in anisotropic conductive adhesive's performance. In this master project, the effects of non-conductive particles as spacers on distribution and deformation of conductive particles in ACA have been investigated. A quantification tool characterize the particle distribution has been developed for ACA application. Pseudorandom model is also a powerful tool that gives guidance for proper particle concentration as well as classify and evaluate an ACA quality.

Results from the project have shown that incorporation of polymeric spacers can be improved by treatment with ethyl acetate solvent. The obtained ACP allow better distribution and more consistent deformation of MPS.

Without UPS, ACP at 1% and 2% volume fraction of MPS, short-circuit failure occurs at spacing of $18\mu m$ and $20\mu m$ respectively. On the contrary, ACP contain 2%vol of MPS and 20%vol of UPS does not short-circuit down to spacing of $18\mu m$. Open-circuit rate of ACP with UPS is, on the other hand, higher than that of ACP without UPS.

Spacing effects using UPS is apparent as particles remain non-crushed under pressure of 18MPa. Without the presence of spacers, MPSs are crushed when the bonding pressure is 12MPa. However, at high pressure, electrical resistance of ACP without spacer is lower than that of ACP with spacer, which might be due to unoptimized spacer size.

Chapter 8

Outlook

The research has shown promising potential for different applications and further studying to be carried out.

The distribution quantification tool are useful in evaluating ACA quality. It can be apply efficiently to the film form ACF. This tool can therefore improve quality control of ACF/ACP in production stage.

Study on spacers in this project has raised new topics for further studies and investigations, including: - Investigate the effect different polymer cores on dispersion of spacer to adhesive matrix, in order to reduce the spacer treating step.

- Characterize the thickness and co-planarity of bonding at different volume fraction of spacers

- Optimize the spacers size for minimum resistance of ACA.

Bibliography

[1] H. Kristiansen, T.O. Gronlund, and J. Liu, "Characterisation of metal-coated polymer spheres and its use in anisotropic conductive adhesive," *Proceedings of the Sixth IEEE CPMT Conference on High Density Microsystem Design and Packaging and Component Failure Analysis (HDP '04)*, pp. 0–4, 2004.

[2] Stephen Westland and Vien Cheung, *Handbook of Visual Display Technology*, 2012.

[3] J.R. Morris, "Interconnection and assembly of LCDs," *Proceedings of Second International Workshop on Active Matrix Liquid Crystal Displays*, pp. 66–71, 1995.

[4] Sun Chul Kim and Young Ho Kim, "Review paper: Flip chip bonding with anisotropic conductive film (ACF) and nonconductive adhesive (NCA)," *Current Applied Physics*, vol. 13, no. 4 SUPPL.2, pp. S14–S25, 2013.

[5] T Osaka, *Electrochemical Technology: Innovation and New Technologies*, Taylor & Francis, 1997.

[6] "Chip-On-Glass (COG) for LCD modules The Chip-on-Glass Concept," .

[7] Rao R. Tummala, *Fundamentals of Microsystems Packaging*, 2001.

[8] H. Kristiansen, Z. L. Zhang, and J. Liu, "Characterization of mechanical properties of metal-coated polymer spheres for anisotropic conductive adhesive," *Proceedings of the International Symposium and Exhibition on Advanced Packaging Materials Processes, Properties and Interfaces*, vol. 2005, pp. 209–213, 2005.

[9] Shuichi Tanaka, Hideo Imai, Haruki Ito, Shinji Mizuno, Nobuaki Hashimoto, and Akira Makabe, "Resin Core Bump Technology for Highly Reliable 20 μ m Pitch Chip on Glass Interconnections," vol. 1, no. 1, pp. 36–39, 2008.

[10] Myung Jin Yim, Jinsang Hwang, and Kyung Wook Paik, "Anisotropic Conductive Films (ACFs) for Ultra-Fine Pitch Chip-On-Glass (COG) Applications," 2005.

[11] Rong-chang Liang, Yasumasa Morita, Scott Tseng, Shuji Rokutanda, Jerry Chung, and Zarng-arh George Wu, "Ultra Fine Pitch Anisotropic Conductive Film with Fixed Array of Conductive Particles," *Science*, pp. 1909–1912, 2010.

[12] Myung Hwan Hong, Sun Chul Kim, and Young Ho Kim, "Ultra-fine pitch chip-on-glass (COG) bonding with metal bumps having insulating layer in the side walls using anisotropic conductive film (ACF)," *Current Applied Physics*, vol. 12, no. 3, pp. 612–615, 2012.

[13] Kyoung-Lim Suk, Chang-Kyu Chung, and Kyung-Wook Paik, "Nanofiber anisotropic conductive adhesives (ACAs) for ultra fine pitch chip-on-film (COF) packaging," *2011 61st Electronic Components and Technology Conference*, , no. 1, pp. 656–660, 2011.

[14] Sang Hoon Lee, Tae Wan Kim, and Kyung-wook Paik, "A Study on Nanofiber Anisotropic Conductive Films (ACFs) for Fine Pitch Chip-on-Glass (COG) Interconnections," pp. 1060–1063, 2014.

[15] Helge Kristiansen, Johan Liu, and Senior Member, "Interconnection Technologies for LCD ' s," vol. 21, no. 2, pp. 208–214, 1998.

[16] Il Kim, Kyung Woon Jang, Ho Young Son, Jae Han Kim, and Kyung Wook Paik, "Wafer-level packages using anisotropic conductive adhesives (ACAs) solution for flip-chip interconnections," *IEEE Transactions on Components, Packaging and Manufacturing Technology*, vol. 1, no. 5, pp. 792–797, 2011.

[17] Hoang Vu Nguyen, *Interconnection Technologies based on Metal-coated Polymer Spheres*, Ph.D. thesis, Univercity of Oslo, 2012.

[18] Bo Tao, Han Ding, Zhouping Yin, and Youlun Xiong, "ACF Curing Process Optimization for Chip-on-Glass (COG) Considering Mechanical and Electrical Properties of Joints," , no. November, 2009.

[19] Xu Chen, Jun Zhang, Chunlei Jiao, and Yanmin Liu, "Effects of different bonding parameters on the electrical performance and peeling strengths of ACF interconnection," *Microelectronics Reliability*, vol. 46, no. 5-6, pp. 774–785, 2006.

[20] J. S. Hwang, M. J. Yim, and K. W. Paik, "Effects of bonding temperature on the properties and reliabilities of anisotropic conductive films (ACFs) for flip chip on organic substrate application," *Microelectronics Reliability*, vol. 48, no. 2, pp. 293–299, 2008.

[21] G. Dou, D. Whalley, and C. Liu, "Mechanical and electrical characterisation of individual aca conductor particles," in *Electronic Materials and Packaging, 2006. EMAP 2006. International Conference on*, Dec 2006, pp. 1–9.

[22] J. S. Hwang, "Filler size and content effects on the composite properties of anisotropic conductive films (ACFs) and reliability of flip chip assembly using ACFs," *Microelectronics Reliability*, vol. 48, no. 4, pp. 645–651, 2008.

[23] Edward M. Petrie, *EPOXY ADHESIVE FORMULATIONS*, 2006.

[24] D.J. Bray, S.G. Gilmour, F.J. Guild, and a.C. Taylor, "The effects of particle morphology on the analysis of discrete particle dispersion using Delaunay tessellation," *Composites Part A: Applied Science and Manufacturing*, vol. 54, pp. 37–45, 2013.

[25] Z. P. Luo and J. H. Koo, "Quantifying the dispersion of mixture microstructures," *Journal of Microscopy*, vol. 225, no. 2, pp. 118–125, 2007.

[26] Srinivasa R. Bakshi, Ruben G. Batista, and Arvind Agarwal, "Quantification of carbon nanotube distribution and property correlation in nanocomposites," *Composites Part A: Applied Science and Manufacturing*, vol. 40, no. 8, pp. 1311–1318, 2009.

[27] Bryan M. Tyson, Rashid K. Abu Al-Rub, Ardavan Yazdanbakhsh, and Zachary Grasley, "A quantitative method for analyzing the dispersion and agglomeration of nano-particles in composite materials," *Composites Part B: Engineering*, vol. 42, no. 6, pp. 1395–1403, 2011.

[28] T. Glaskova, M. Zarrelli, a. Borisova, K. Timchenko, a. Aniskevich, and M. Giordano, "Method of quantitative analysis of filler dispersion in composite systems with spherical inclusions," *Composites Science and Technology*, vol. 71, no. 13, pp. 1543–1549, 2011.

[29] H G Merkus, *Particle Size Measurements: Fundamentals, Practice, Quality*, Particle Technology Series. Springer Netherlands, 2009.

[30] DAVID J WILLIAMS and DAVID C WHALLEY, "The effects of conducting particle distribution on the behaviour of anisotropic conducting adhesives: non-uniform conductivity and shorting between connections," *Journal of Electronics Manufacturing*, vol. 03, no. 02, pp. 85–94, 1993.

[31] D E Packham, *Handbook of Adhesion*, Wiley, 2006.

[32] I Smallwood, *Handbook of Organic Solvent Properties*, Elsevier Science, 2012.

Publication

Quantification of Particle Distribution in Anisotropic Conductive Adhesive

Huyen T. Nguyen, Knut E Aasmundtveit, Helge Kristiansen,
Hoang-Vu Nguyen, Giang M. Nghiem,
Erik Kalland and Susanne Helland

Proceeding to IMAPS Nordic 2016 Annual Conference

Quantification of particle distribution in anisotropic conductive adhesive

Huyen T. Nguyen[1], Knut E Aasmundtveit[1], Helge Kristiansen[2], Hoang-Vu Nguyen[1], Giang M. Nghiem[1], Erik Kalland[2] and Susanne Helland[2]

[1]HSN –University College of Southeast Norway, Raveien 197, N-3184 Borre, Norway
[2]Conpart AS, Dragonveien 54, N-2013 Skjetten, Norway

Phone: +47 98816695 Email: Huyen.Nguyen@student.hbv.no

Abstract

The distribution of conductive particles in the matrix plays a crucial role in ACA fine/ultra-fine pitch applications. This study developed a method for quantitative evaluation of particle distribution, which includes clusterization and dispersion. Clusterization parameter C and dispersion parameter D are measured by statistical calculation of clusters/particles' size in the matrix and sub-region particle area fraction respectively. Sensitivity of the method to different distribution patterns was high, compared to other methods, providing a good evaluation and classification of how well particles distribute in ACA. Results from applying the methods to real ACA bonding also show an agreement between ACA distribution and electrical failure rate.

Key words: Anisotropic conductive adhesive, metal coated polymer sphere, distribution quantification, clusterization, dispersion

1. Introduction

Anisotropic conductive adhesives (ACAs) is conductive in z-axis forming interconnects between chips and substrates while isolating adjacent interconnects in xy-plane. An ACA usually contains mono-sized metal-coated polymer spheres (MPSs) incorporated in an adhesive matrix. The conducting mechanism of ACA is shown in Figure 1. Conductive particles are trapped and deformed between bumps on chips and pads on substrate, thus allowing vertical electrical conduction. The likelihood of trapping conductive particles is strongly correlated with the bump size. Particles in the space between two bumps are isolated by the adhesive matrix, preventing short-circuit between adjacent bumps. Two typical failure modes of ACA bonding exist: short-circuits between adjacent bumps and open-circuit within interconnects. Clusters of particles with size larger than the minimum spacing between bumps can cause short-circuits while a non-uniform dispersion might lead to the latter failure mode. Therefore, distribution of these particles in the matrix plays a significant role in ACA fine/ultra-fine pitch applications. A tool to quantify the particle distribution is therefore essential for characterization of the ACAs prior to the bonding process.

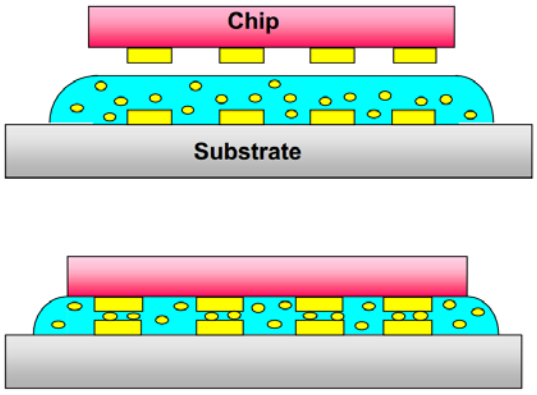

Figure 1: 1 Working principle of ACA [1]

Several methods have been proposed for quantifying nano-particle distribution in composite materials [2-5]. A dispersion parameter called Area Disorder was used by David J. Bray, et al [2] to quantitatively classify the dispersion of particles as good, random or poor. Images of the material was divided into a triangle network, where each vertex of a triangle is a particle and no particle is found inside a triangle or on its edge. An Area Disorder is then defined based on the ratio between mean of triangle areas and their standard deviation. This method however does not provide any evaluation on agglomeration of the particles.

Luo & Koo [3] calculated dispersion quantity *D* based on measurement of distances between particles. *D* is a percentage value, higher *D* means better dispersion of particles. B.M. Tyson et al [4] improved the method by adding quantification of agglomeration. Characterized properties are the size of fillers/clusters and distances between them in x and y direction. The method proposed by T.Glaskova et al [5] focused on studying the agglomeration/ clusterization of particles by similar calculation on

area of clusters. Since distribution parameters quantified are percentage values, these methods can provide a good insight of how well filler particles disperse or agglomerate into the composite matrix.[4] However, short-circuiting in ACA bonding is caused by clustering of particles in any direction. Study of cluster size in one direction or cluster area does not related directly to possibility of this failure. Similarly, distances between particles only have a weak relation to open-circuit failure. Therefore, in order to utilize these methods in evaluation of ACA particle distribution, further improvement need to be made.

In this work, a methodology is proposed to quantify the distribution of the mono-sized particles in the ACA. A clusterization parameter C_k is found based on maximum cluster size while the dispersion parameter D_k is related to particle area fraction in sub-regions of the matrix. To validate the method, three different types of images were generated and quantified. They are: computer generated images; images taken from real ACA bonding between flat substrates and dies; and images taken from real ACA bonding between bumped substrates and flat dies. Sensitivity of distribution parameters will then be evaluated based on different distribution patterns. Comparison between flat samples and bumped samples relating to ACA failure rate will also be presented.

2. Methods for particle distribution quantification

2.1. Previous quantification methods

Figure 2 describes the procedure of obtaining dispersion parameter *D* and agglomeration parameter *A* suggested in [3] and [4]. A gridline network in x and y direction is first created on the image under consideration. Data of white segments on the gridlines is recorded as free-path spacing x_D while black segments represent filler agglomeration sizes x_A. Histograms of the two data sets (x_D and x_A) are plotted and fitted to either normal or lognormal distribution. From the fitted curve, a probability density function $f(x)$ is obtained and the dispersion parameter D_k and the agglomeration parameter A_k are calculated. D_k and A_k are related to the probability of x falling in a certain range k around the mean value μ of x, i.e. the integration of $f(x)$ from $(1-k)\mu$ to $(1+k)\mu$:

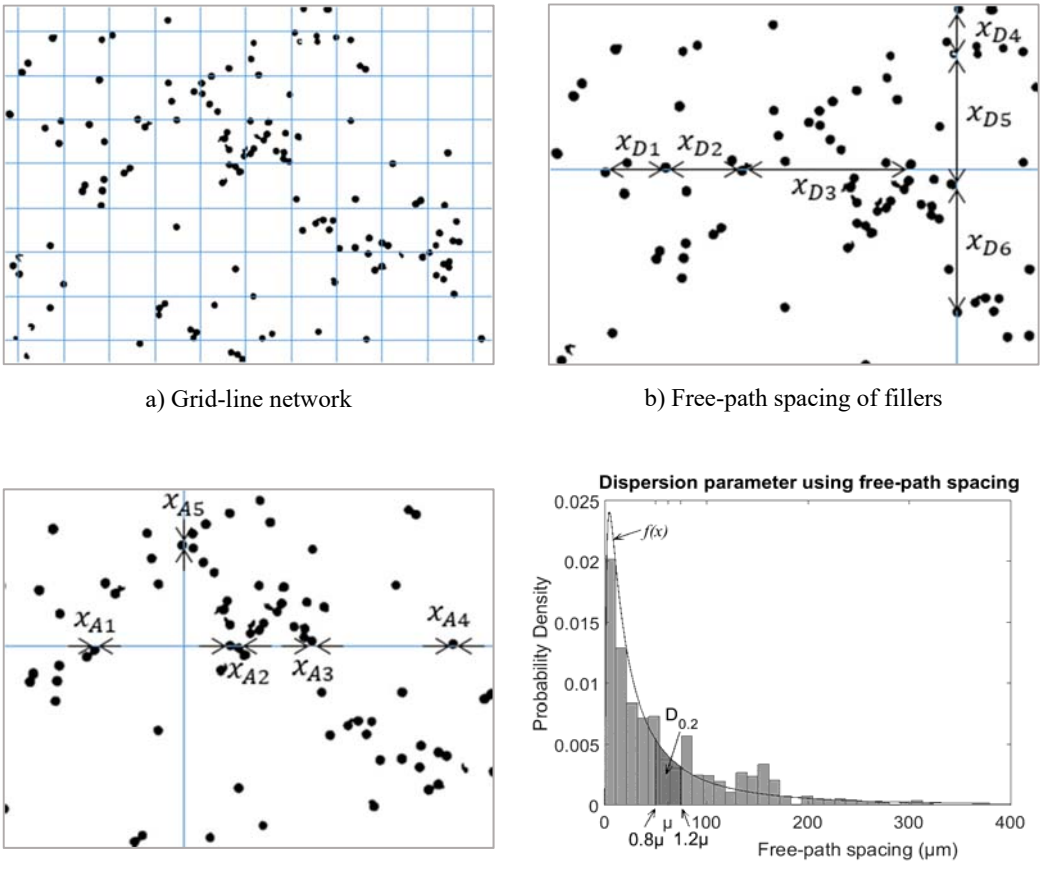

a) Grid-line network

b) Free-path spacing of fillers

c) Agglomeration sizes of fillers

d) Calculation of dispersion parameters

Figure 2: Determination of distribution parameters. First, a gridline network is made on the image (a). On each line, white segments representing particle spacing (b) while black segments represent particle sizes are measured and histogram of them are plotted. In (d), histogram of particle spacing is plotted and a lognormal curve are fitted. $D_{0.2}$ is the shaded area under the fitting curve, where μ is the mean value of particle spacing.

$$D_k = \int_{(1-k)\mu_{x_D}}^{(1+k)\mu_{x_D}} f(x_D)\mathrm{d}x_D \quad (1)$$

while $$A_k = 1 - \int_{(1-k)\mu_{x_A}}^{(1+k)\mu_{x_A}} f(x_A)\mathrm{d}x_A \quad (2)$$

$0 < k < 1$ and k is chosen in such way that $f(x)$ in the considered range is linear.

We have: $$\int_0^\infty f(x)dx = 1 \quad (3)$$

Therefore, $0 < D_k < 1$ and $0 < A_k < 1$. B.M. Tyson et al [4] proved that the larger D_k is, the narrower the statistical distribution of x_D is, thus the more uniform the dispersion of fillers in the matrix is. While A_k is set up in such a way that smaller A_k indicates less agglomeration.

T.Glaskova's work [5] focused on studying the agglomeration/clusterization of particles by similar calculation on areas of clusters. Normal distribution was fitted to the data.

2.2. A modified method for ACA application

There exist very few published works on the particle distribution in ACA. Therefore, a tool for quantifying and evaluating ACA particle distribution is of apparent necessity. In this paper, a method for quantification of mono-sized particle distribution in an adhesive matrix was adapted from previous methods with improvement and modification. For sufficient quantifying the distribution of ACA particles, there is a need of analyzing both parameters for clusterization and dispersion of the particles.

For quantification of clusterization, clusters and cluster size were first defined. A cluster is defined as a group of particles having physical contacts that can provide continuous conduction paths from any particle to all the other particles within the group. The size F of a cluster is its maximum Feret diameter, where Feret diameter is the distance between two parallel tangents on opposite sides of the cluster [7], as shown in Figure 4. Thus, two neighbor bumps with spacing smaller than size of a cluster have a possibility of being short-circuited by that cluster.

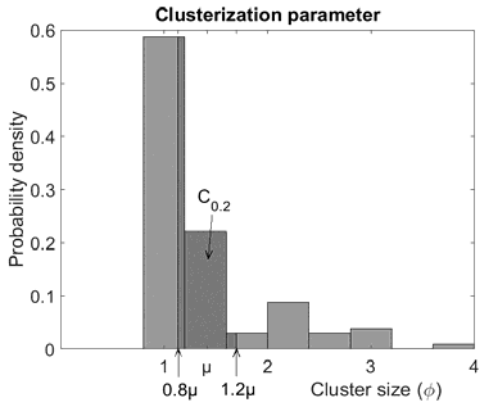

Figure 3: Clusterization parameter definition

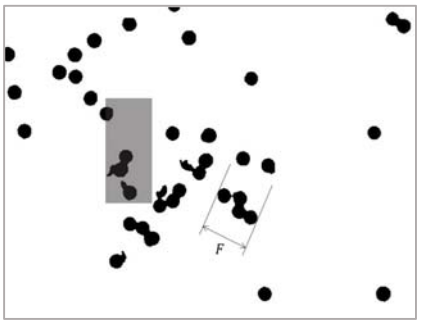

Figure 4: Feret diameter F and shaded rectangle for calculation of sub-region area-

Separated single particles are considered as clusters with size equals to their diameter. Since this study focuses on mono-sized particles, the cluster size unit is one particle diameter, denoted as ϕ.

Similar to previous method, the clusterization parameter C_k is related to the statistical distribution of cluster sizes F. However, since the ACA particle distribution has not been studied carefully, it is not reasonable to fit the statistical distribution of cluster size to any laws of distribution in advance. Therefore, we used the discrete histogram (Figure 3) of real measured values to extract C_k, which is then defined as the ratio of total number of clusters with size fall in the range of $(1-k)\mu_F$ to $(1+k)\mu_F$ over total number of clusters in the image, where μ_F is the mean cluster size.

$$C_k = \frac{\sum_{(1-k)\mu_F}^{(1+k)\mu_F} N(F)}{\sum_0^{Fmax} N(F)} \quad (4)$$

$0 \le C_k \le 1$ and C_k can be expressed in percentage value. For ACA application, where the area fraction of particle is mainly smaller than 15%, most of clusters in an image are single particles and mean cluster size μ_F is close to 1ϕ. The existence of large clusters increases μ_F further from 1ϕ as well as widens the statistical distribution of cluster size, thus considerably decreases C_k. An image with only single particles has $C_k = 1$ while $C_k \approx 0$ if an image contains clusters with size varying greatly. Therefore,

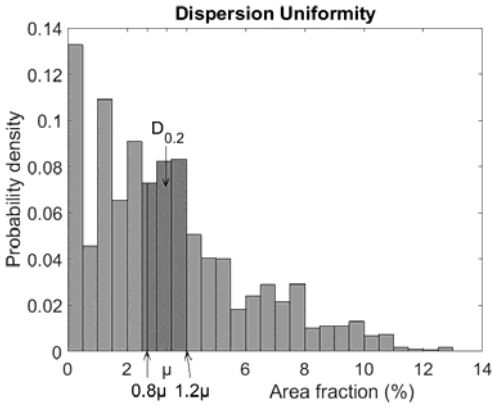

Figure 5: Dispersion parameter definition based on sub-region area fraction *a*

C_k can express well the degree of particle clustering, the larger C_k is, the less clustering between particles s.

Non-uniform dispersion of the particles/ clusters may lead to areas with insufficient particles to conduct in z-direction. Clusterization parameter does not take into account this tendency of particle dispersion. Free-path spacing property as in mentioned methods can be used to characterize dispersion of particles. However, in order to fit better the requirement of ACA, a different property is proposed when quantifying dispersion parameter, which is the sub-region area fraction a. Shaded rectangle in Figure 4 represent a sub-region of interest, which can be consider as a bump to connect. Area fraction a on this bump is the ratio between particle covered area over the area of the bump.

$$\boldsymbol{a = \frac{Bump\ area\ covered\ by\ particle}{Total\ bump\ area}} \qquad (5)$$

This bump is moving with a small step through the whole image, collecting area fraction a in each position. Histogram of recorded data is plot as in Figure 5 indicating how uniform the area fraction a is over the whole image. Identical calculation for C_k is apply to dispersion parameter D_k, with area fraction a replacing cluster size F.

$$\boldsymbol{D_k = \frac{\sum_{(1-k)\mu_a}^{(1+k)\mu_a} N(a)}{\sum N(a)}} \qquad (6)$$

Similar to C_k, $0 \leq D_k \leq 1$. $D_k = 1$ means perfectly uniform dispersion of particles. The larger D_k is, the better the uniformity of spreading particles over the matrix is.

3. Experimental

For accurately measuring distribution parameters, clear binary images are needed. ACAs come with two typical forms: paste (ACP) and film (ACF). In our work, we studied adhesive pastes with epoxy matrix and mono-sized (very narrow size distribution) MPSs of 5µm in diameter as conductive particles. Nevertheless, the method can be used in both cases if single layered images are acquired.

Mixing of an ACP starts with mixing of epoxy and hardener by speed mixer, MPSs are then incorporated together with a thixotropic agent to prevent the sedimentation of the MPS. To obtain a single particle layer, the adhesive was squeezed to a single layer between two substrates, one of which is glass, using a FinePlacer flip-chip bonder. The other

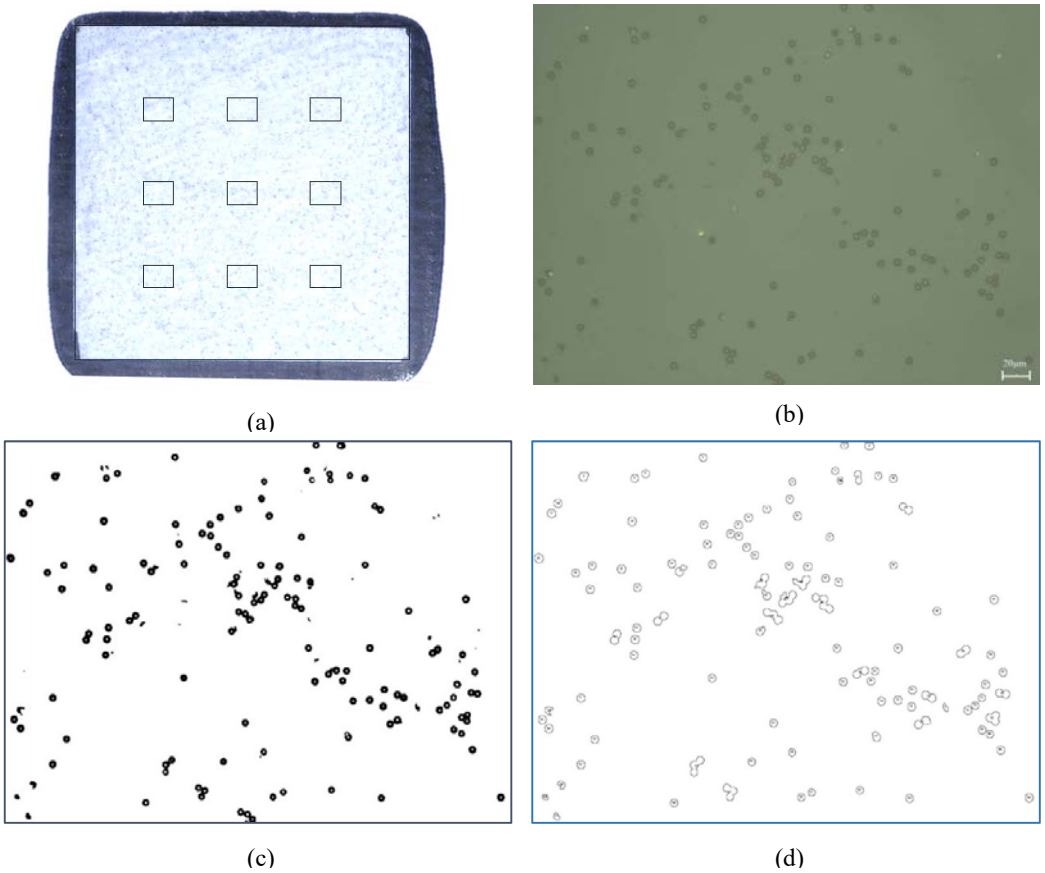

Figure 6: Procedure of obtaining, processing and analyzing images. ACA bond is made (a) and positions for taking microscope images are determined. These images (b) is then thresholded (c) and analyzed (d) using ImageJ freeware.

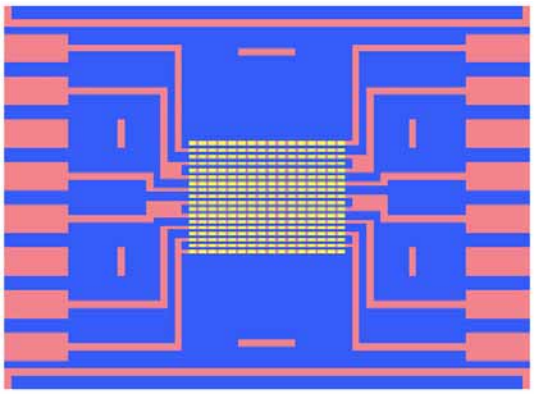

Figure 8: Design of the patterned substrate. Pink pads and wires (of 1µm high) are for electrical measurement while yellow rectangles (10µm) are bumps where particles are trapped. Particle clustering in the space two bump rows can cause short-circuit and can be detected.

part is either a small glass die or a silicon substrate with gold-covered copper bumps. Bonding process is conducted at 160°C for 30s under a pressure of 1.25MPa.

The procedure for analyzing the flat (glass-glass) samples are shown in Figure 6. Images taken at 9 well defined positions (a) on the samples are captured using optical microscope (Figure 6b). Each image is then processed (c) and analyzed using ImageJ software (d). Feret diameter of each cluster is recorded and further investigation is carried out on the binary images (c).

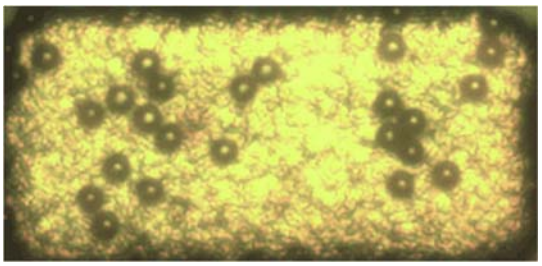

Figure 7: Surface of a bump with trapped particles. *a'* is then determined based on these images, which is the ratio of particle covered area and bump area

Patterned samples made of comb-like structures consisting of interleaved fingers were designed to evaluate the insulation properties of the ACA. Two kinds of patterned samples were used, one with set of gap spacing between fingers is 35-40-45µm and one with 18-20-22 µm. Figure 8 shows design of first kind. Each finger of this sample consists of 16 connected bumps with dimensions length×width×height of 100µm×50µm×10µm. After bonding with ACP, electrical testing were used to detect any insulation failure in the samples. Failure is considered as when the resistance of the adhesive in the gaps between fingers is smaller than 1GΩ.

Optical microscope images of bumps' surface (Figure 7) are then taken and the real particle-covered area fraction of bumps are analyzed. A bump with less than 1.18% area covered (corresponding to 3 particles of 5µm in diameter cover a 50µm×100µm

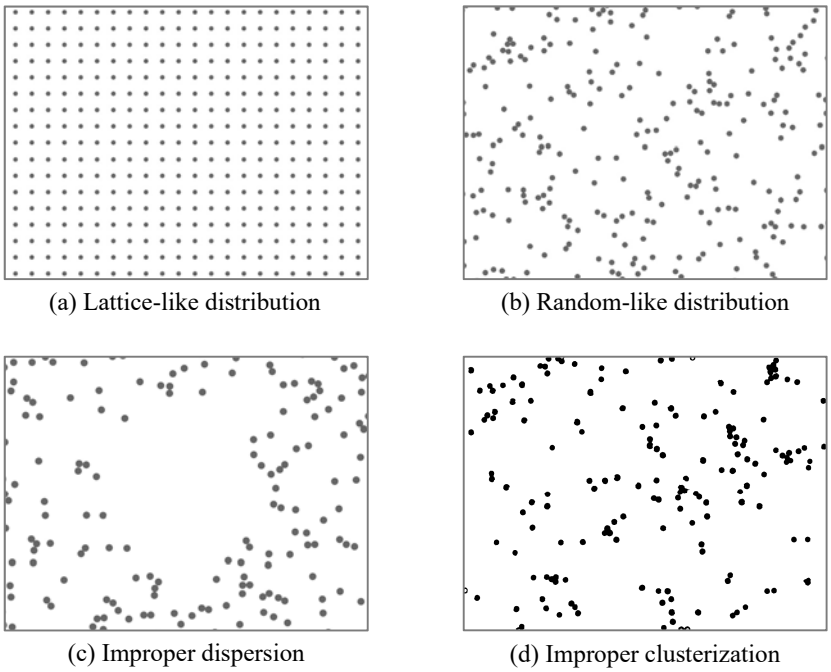

(a) Lattice-like distribution

(b) Random-like distribution

(c) Improper dispersion

(d) Improper clusterization

Figure 9: Examples of different particle distribution, from ideal to improper distribution

bump) are considered as an open interconnect. Open-circuit rate is then estimated.

4. Comparison of different methods

To evaluate the sensitivity of different distribution parameters, images of four distinct distribution of same particle concentration were studied, as in Figure 9: (a) lattice-like, (b) random-like, (c) bad dispersion with unoccupied area and (d) real ACA bonding with apparent clusterization. Analyzed results of each image are displayed by Table 1 and Table 2. $k = 0.2$ was used for both C_k and D_k.

Table 1 shows dispersion parameters obtained from previous method, using free path spacing for calculation, and the modified method, using sub-region area-fraction for calculation. As displayed, two methods agree well for the first three samples (a) to (c). For lattice-like distribution (a) with particles evenly arranged through out the image, D_k for both cases is close to 1. These parameters of both methods dropped significantly for random-like distribution and decrease further for distribution with big unoccupied area in (c). However, when comparing (c) and (d), the two methods do not agree. First method indicates that (c) has better dispersion while second method claim the contrary. In (c), apart from the unoccupied area, particles are dispersed reasonably well. On the other hand, particle spacing in (d) falls into a very wide range. However, using sub-region area fraction, the big empty area in (c) decreases D_k to less than that value of (d). It is insufficient to conclude which method is better but for ACA application, distribution as in (d) is of preference. The empty area in (c) contains an ineligible possibility of open-circuit failure. Thus, D_k from modified method is more suitable to evaluate the dispersion of particles in ACA bonding.

Table 1: Dispersion parameters, $D_{0.2}$

Example	Free-path spacing	Sub-region area fraction
a	0.94	1.00
b	0.15	0.30
c	0.14	0.20
d	0.12	0.22

Three parameters representing the particle clustering are considered: clustering parameters, mean and standard deviation of cluster sizes. The three parameters agree well with each other in all cases, indicating that there is no clustering for (a), clustering to some extent in (b) and (c), and notable clusterization in (d). The sensitivity of each parameter is, on the other hand, different. Comparison between the two cases b and d, $C_{0.2}$ remarkably decreased by 4 times while μ and σ increased 1.6 and 2.4 times respectively. Thus, this parameter $C_{0.2}$ is more sensitive to the degree of clustering than μ and σ. Furthermore, since C_k is a percentage value, it can show how serious the clusterization of particle is compare to the ideal case and worst case.

Table 2: Clusterization parameters

Ex	$C_{0.2}$	Mean μ [ϕ]	Standard deviation σ [ϕ]
a	1.00	1.00	0.00
b	0.88	1.19	0.40
c	0.85	1.23	0.41
d	0.23	1.96	0.97

(1ϕ = 1 particle diameter)

5. Application of method in ACA bonding

To verify the method in ACA applications, bonding of 2 ACPs with different MPS volume fraction (1%vol and 3%vol) on blank and patterned samples were made. Results are detailed in Table 3 and Table 4.

For clusterization properties of ACPs, C_k values of both adhesives were low, indicating a distribution that is far from random. Smaller value was seen in higher concentration of MPS.

Detected short-circuiting failures are as expected since the histograms of cluster size on blank samples show a possibility of short-circuiting at these gap spacing.

Table 3: Clusterization of MPS

Properties		1%vol	3%vol
Blank samples	μ_F [μm]	8.74	10.67
	$C_{0.2}$	0.23	0.17
	% large clusters	1.38% F > 18 μm	0.94% F > 40 μm
Bumped samples	Short-circuit	21% at spacing 18 μm, length 5600μm	22% at spacing 40 μm, length 1600μm

Comparison of particle dispersion properties between blank samples and patterned samples shows some differences but there is a consistence between two ACPs.

Mean values of area fraction in blank glass samples are higher than that in patterned samples. Bonding was carried out using flip-chip bonder, in which, blank die is bonded on top of the patterned substrate. This means that highest places on the substrates are bumps' surface, this lead to less particle are trapped on bumps. However, the statistical distribution of area fraction covered by particles on bumps a' are better than a (as defined earlier) of blank samples. $D_{0.2}$ values of a and a' indicate that particles dispersion on bumps area more uniform than on blank samples. Histograms plot in Figure 10 and Figure 11 also present a narrower span of a' values. However, the modes of a and a' in both histograms, i.e. the most frequent value in a data set, is close to each other in both cases.

Open-circuit rate predicted by blank samples are also higher than real samples, indicating that prediction from blank samples are safe.

Table 4: Dispersion of MPS

Properties		1%vol	3%vol
Blank glass samples	μ of area fraction (%)	7.05	14.36
	$D_{0.2}$	0.20	0.26
	Open-circuit rate predicted (%)	8.47	2.03
Bumped samples	μ of area fraction (%)	3.07	9.17
	$D_{0.2}$	0.23	0.31
	Open-circuit rate (%)	4.86	0.17

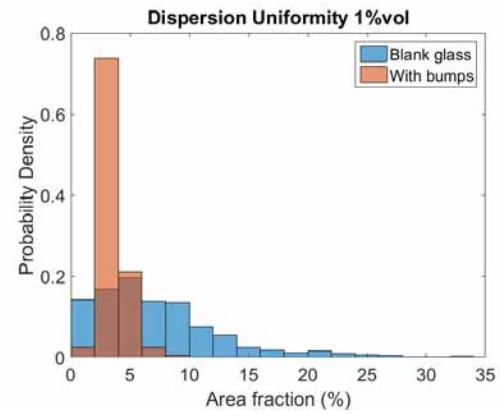

Figure 10: Histogram of *a* and *a'* for 1%vol ACP

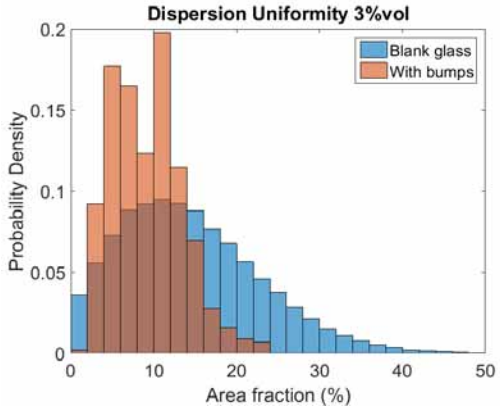

Figure 11: Histogram of *a* and *a'* for 3%vol ACP. *a* (blue): particle area fraction in sub-regions of blank samples, *a'*(red): particle area fraction on bumps of patterned samples

6. Conclusion

A methodology for distribution measurement of mono-sized spherical particles in a matrix were developed. The proposed method is suitable for evaluating ACA quality. Parameters of clusterization C_k and dispersion D_k were defined based on measurement of cluster size and sub-region area fraction. The results show that these parameters are significantly more sensitive to different distributing patterns compared to other methods, such as ….

Comparison between bonds of blank glass samples and patterned samples showed that C_k and D_k can be used directly to evaluate the quality of an ACP. The obtained results prove that blank sample bonds are able to safely predict failure rate of real patterned sample bonds. Thus, this provide a tool to evaluate the quality of ACP before real bonds on patterned samples taking place.

7. References

Journal article

[1] H. Kristiansen, Z. L. Zhang, and J. Liu, "Characterization of mechanical properties of metal-coated polymer spheres for anisotropic conductive adhesive," *Proc. Int. Symp. Exhib. Adv. Packag. Mater. Process. Prop. Interfaces*, vol. 2005, pp. 209–213, 2005.

[2] Bray, D. J., Gilmour, S. G., Guild, F. J., & Taylor, A. C. (n.d.). Estimating nanoparticle dispersion using the Area Dis- order of Delaunay triangulation. *Journal of the Royal Statistical Society Series C - Applied Statistics,* vol. 61, 2012

[3] Luo, Z. P., & Koo, J. H. (2007). Quantifying the dispersion of mixture microstructures. *Journal of Microscopy*, *225*(2), 118–125.

[4] Tyson, B. M., Abu Al-Rub, R. K., Yazdanbakhsh, A., & Grasley, Z. (2011). A quantitative method for analyzing the dispersion and agglomeration of nano-particles in composite materials. *Composites Part B: Engineering*, *42*(6), 1395–1403.

[5] Glaskova, T., Zarrelli, M., Borisova, a., Timchenko, K., Aniskevich, a., & Giordano, M. (2011). Method of quantitative analysis of filler dispersion in composite systems with spherical inclusions. *Composites Science and Technology*, *71*(13), 1543–1549.

[6] Williams, D. J., & Whalley, D. C. (1993). The effects of conducting particle distribution on the behaviour of anisotropic conducting adhesives: non-uniform conductivity and shorting between connections. *Journal of Electronics Manufacturing*, *03*(02), 85–94.

Book

[7] Merkus, H. G. (2009). *Particle Size Measurements: Fundamentals, Practice, Quality*. Springer Netherlands.